

Brain-specific deletion of histone variant H2A.z results in cortical neurogenesis defects and neurodevelopmental disorder

Tianjin Shen^{1,2}, Fen Ji^{1,2}, Yuanyuan Wang^{1,2}, Xuepei Lei^{1,2}, Dongming Zhang^{1,2} and Jianwei Jiao^{1,2,*}

¹State Key Laboratory of Stem Cell and Reproductive Biology, Institute of Zoology, Chinese Academy of Sciences, Beijing 100101, China and ²University of Chinese Academy of Sciences, Beijing 100049, China

Received July 12, 2017; Revised December 04, 2017; Editorial Decision December 14, 2017; Accepted December 19, 2017

ABSTRACT

Defects in neurogenesis alter brain circuit formations and may lead to neurodevelopmental disorders such as autism and schizophrenia. Histone H2A.z, a variant of histone H2A, plays critical roles in chromatin structure and epigenetic regulation, but its function and mechanism in brain development remain largely unknown. Here, we find that the deletion of *H2A.z* results in enhanced proliferation of neural progenitors but reduced neuronal differentiation. In addition, neurons in *H2A.z* knockout mice exhibit abnormal dendrites during brain development. Furthermore, *H2A.z*^{CKO} mice exhibit serial behavioral deficits, such as decreased exploratory activity and impaired learning and memory. Mechanistically, H2A.z regulates embryonic neurogenesis by targeting *Nkx2-4* through interaction with Setd2, thereby promoting H3K36me3 modification to activate the transcription of *Nkx2-4*. Furthermore, enforced expression of *Nkx2-4* can rescue the defective neurogenesis in the *H2A.z*-knockdown embryonic brain. Together, our findings implicate the epigenetic regulation by H2A.z in embryonic neurogenesis and provide a framework for understanding how disruption in the *H2A.z* gene may contribute to neurological disorders.

INTRODUCTION

During embryonic neurogenesis, neurons are generated from neural progenitor cells (NPCs) directly or indirectly in a spatially and temporally regulated manner (1,2). These postmitotic neurons form functional neuronal circuits after migrating over a long distance to their final locations (3). Any disturbance in this process of neurogenesis might result in neurodevelopmental disorders, including schizophrenia

and autism (4–6). Besides transcription factors, epigenetic molecules also play a crucial role in the spatial and temporal control of cortical neurogenesis (7–10). Posttranslational modifications of histone proteins affect the access of transcription factors to target sites, contributing to the complex control of gene expression (11,12). An additional regulatory mechanism is the replacement of conventional histones with their specific variants within the chromatin (13,14).

Histone variants are structural components of chromatin and have evolved crucial roles in genome integrity, transcriptional regulation, DNA repair, and other processes (15). Among those variants, H2A.z is of particular interest with respect to its function (16–18). H2A.z belongs to the H2A family but has only 60% identity to canonical H2A (19). Recent studies in various cellular systems show that H2A.z also has multiple functions in the transcription process, including transcriptional activation, repression, and elongation (17,20–23). Moreover, deficiency of *H2A.z* leads to embryonic lethality at the pre-implantation stage of the blastocyst (24). Interestingly, H2A.z has apparently contradictory roles in gene activation and silencing (18,25,26). Some of these contradictions might be explained by local histone modification patterns (25). In addition, a genome-wide linkage study indicated that the *H2A.z* gene may be a susceptibility factor for schizophrenia (27). Schizophrenia comprises a range of neurodevelopmental disorders characterized by mental disorder, delusions and cognitive deficits, with highly heritability (28). Therefore, it is particularly important to illustrate how H2A.z incorporation alters chromatin states to regulate gene expression during embryonic neurogenesis.

Although there is a wide consensus on the importance of *H2A.z*, the function of H2A.z in embryonic neurogenesis and animal behavior remains unknown. Here, we report that the deletion of *H2A.z* not only promotes the proliferation of progenitors but also inhibits neuronal differentiation. Neurons in *H2A.z* knockout mice exhibit abnormal dendrites with cortical development. Mechanisti-

*To whom the correspondence should be addressed. Tel/Fax: +86 10 64806335; Email: jwjiao@ioz.ac.cn

cally, H2A.z regulates the expression of Nkx2-4 by interaction with Setd2, thereby promoting the H3K36me3 levels of the promoter. The combination of H2A.z and histone H3K36me3 modification by Setd2 promotes transcriptionally permissive chromatin and transcriptional activation in the developing brain. In addition, *H2A.z^{CKO}* mice exhibit decreased exploratory activity and social behavior and impaired learning and memory, and they are prone to anxiety and depression. Together, our study reveals the functions of H2A.z in progenitor proliferation and differentiation, neuronal morphology, and mice behavior, thus providing new insights into the epigenetic regulation by *H2A.z* in the developing brain.

MATERIALS AND METHODS

Animals

H2A.z1/2 floxed mice were provided by the RIKEN BRC through the National Bio-Resource Project of the MEXT. To generate *H2A.z^{fl/fl}* mice, H2A.z1/2 floxed mice were crossed with C57BL/6J mice, and then the F1 offspring were crossed with each other to obtain *H2A.z1^{fl/fl}* mice. *Nestin-Cre* mice (B6. Cg-Tg(Nes-cre)1Kln/J) were obtained from the Jackson Laboratory. To generate *H2A.z^{CKO}* mice (*H2A.z1^{CKO}* is regarded as *H2A.z^{CKO}* in our study), *H2A.z1^{fl/fl}* mice were crossed with *Nestin-Cre* mice. Genotyping for *H2A.z1* and *Cre* alleles was performed by PCR analysis of tail DNA. All animal experiments were conducted in accordance with the guidelines of the Animal Care and Use Committee of the Institute of Zoology, Chinese Academy of Sciences.

Plasmid constructs

ShRNAs for the target genes were cloned into the pSicoR-GFP vector. The sequences were as follows: *H2A.z*-shRNA1: 5'-GGTAAGGCTGGAAAGGACT-3' (25); *H2A.z*-shRNA2: 5'-CGGGAAGAAAGGACAACAGAA-3' (26); *SETD2*-shRNA: 5'-GAAACCGTCTCCAGTCTGT-3' (29); and *NKX2-4*-shRNA: 5'-CCAGAACCATCGCTACAAGAT-3'; *H2A.v*-sh1: 5'-GTGTTGGAGTTAGCAGGTAAT-3'. The cDNA of *H2A.z*, *siRNA*-resistant *H2A.z* mutant, *H2A*, and *NKX2-4* were amplified by polymerase chain reaction (PCR) and subcloned into the pCDH-3xFLAG vector. *SETD2-SET* domain cDNA was amplified and subcloned into pCDH-3xHA. The *H2A.z*-shRNA1-resistant *H2A.z* cDNA mutant: forward 5'-TAGAGCTGGCGGCAAAGCCGGGAAAGATTCCGGAAAGGC-3'; reverse 5'-GCCTTTCCGGAATCTTTCCCGGCTTTGCCGCAGCTCTA-3'; *SETD2-SET* domain cDNA: forward 5'-GGAATTCGGCAAGTACCAGATTCTCTAACA-3'; reverse 5'-CGGGATCCCTCTTCCACAGTGACAGTCTCTAA-3'.

Cell cultures

Both the cell lines and the primary neural progenitor cells were cultured as previously described (30). Briefly, mouse neuroblastoma N2a cells and the human embryonic kidney (HEK) 293FT cell line were cultured in DMEM (Life

Technologies) supplemented with 10% FBS, GlutaMAX (Invitrogen, 0.5%), nonessential amino acids (Invitrogen, 1%), and antibiotics. Neural progenitor cells were isolated from the dorsal brains of E12 embryos and then cultured in proliferation or differentiation media for subsequent treatment. For primary neurosphere assays, neural progenitor cells were cultured in non-adherent conditions at a clonal density of 50 cells per ml in six-well plates, and neurospheres were counted 3 days later.

In-utero electroporation

In-utero electroporation was performed as previously described (31). Briefly, pregnant mice at E13 were anesthetized, and plasmid DNA and 0.02% Fast Green (Sigma) were microinjected into the lateral ventricle with a glass micropipette. The electroporated brains were removed by dissection at the indicated days and were cut into sections for further analysis.

BrdU labeling

Generally, BrdU was injected intraperitoneally into E15 or E16 pregnant mice at a dose of 100 mg/kg. For cell proliferation analysis, BrdU was injected 2 h before pregnant mice were sacrificed at E16. For cell cycle exit analysis, BrdU was administered at E15 before the pregnant mice were harvested at E16.

Immunostaining

The procedure for immunostaining brain sections or cultured cells was described previously (32). The following antibodies were used: rat anti-BrdU (1:1000; Abcam; ab6326), rabbit anti-Ki67 (1:1000; Abcam; ab15580), rabbit anti-phospho-Histone H3 (pH3) (1:1000; Cell Signaling Technology; 3377S), mouse anti-Nestin (1:200; Millipore; MAB353), rabbit anti-Pax6 (1:1000; Abcam; ab5790), mouse anti-Pax6 (1:100; DSHB), rabbit anti-Tbr2 (1:1000; Abcam; ab23345), mouse anti-Sox2 (1:1000; R&D; MAB2018), rabbit anti-Tuj1 (1:1000; Sigma; T2200), mouse anti-Tuj1 (1:2000; Millipore; MAB1637), rabbit anti-H2A.z (1:1000; Active Motif; 39943), rabbit anti-NeuN (1:1000; Abcam; ab177487), rabbit anti-Nkx2-4 (1:1000; Abcam; ab189202), mouse anti- β -actin (1:2000; Proteintech; 60008-1-Ig), rabbit anti-Flag (1:1000, Sigma; F1804), rabbit anti-IgG (1:1000, Bioss; bs-0295p), mouse anti-HA (1:1000; Abmart; M20003L), rabbit anti-H3K36me3 (1:1000; Cell Signaling Technology; 4909S), rabbit anti-H3K36me3 (Active Motif; 61101), rabbit anti-H3K27me3 (1:1000; Millipore; 07-449), rabbit anti-H3K9me3 (1:1000; Millipore; 07-442), rabbit anti-H3K4me3 (1:1000; Millipore; 07-473), and rabbit anti-H2A (1:500; Proteintech; 10445-1-AP). The secondary fluorescence antibodies used are listed below: Alexa Fluor 488, Cy3, or Cy5 (1:1000; Jackson ImmunoResearch). DAPI (2 μ g/ μ l; Sigma; D9542) was used for nuclear counterstaining.

Western blotting and immunoprecipitation

Western blot analysis and immunoprecipitation were performed as previously described (30). Briefly, protein ex-

tracts were obtained by lysing cells/tissue in RIPA (Solarbio) buffer supplemented with protease inhibitors. For western blotting, protein extracts were separated by SDS-PAGE and transferred onto PVDF or NC membranes, followed by blotting with various antibodies. The bands were visualized using 800CW Donkey-Anti-Rabbit or Donkey-Anti-Mouse IgG as well as 680LT Donkey-Anti-Rabbit IgG or Donkey-Anti-Mouse IgG (LI-COR Biosciences) and the software Odyssey V3.0. For immunoprecipitation studies, protein extracts were incubated with anti-HA-tag magnetic beads (MBL) or anti-Flag-tag magnetic beads (MBL) overnight at 4°C. After washing six times with cold wash buffer, the bound proteins were subjected to western blot analysis.

Lentivirus production and infection

The detailed procedure for lentivirus preparation was described previously (31). For lentivirus infection, MOI (multiplicity of infection) was set to 5, and the incubation time was 12 h. After infection, neural progenitor cells were cultured continually and used for further analysis.

RNA-sequencing analysis

Total RNA was extracted from E13 telencephalic tissue of *H2A.z^{cKO}* and *H2A.z^{fl/fl}* mice. Then, total RNA was quality controlled and quantified using an Agilent 2100 Bioanalyzer. After converting to cDNA and building the library, high-throughput sequencing was performed using the Illumina HiSeq 2500 platform in Annoroad Genomics. The data have been deposited in NCBI's GEO and are accessible through GEO Series accession number GSE99347.

MNase digestion assay

The assay was performed as previously described (33). In brief, cell nuclei were isolated using hypotonic buffer (10 mM HEPES, pH 7.9, 10 mM KCl, 1.5 mM MgCl₂, 0.34 M sucrose, 10% glycerol, and 1 mM dithiothreitol (DTT)) and 0.1% Triton X-100. After washing in hypotonic buffer without Triton X-100, the cell nuclei were resuspended in reaction buffer (15 mM Tris-HCl, pH 7.4, 60 mM KCl, 0.25 M sucrose, 1 mM CaCl₂, and 0.5 mM DTT). The digestion was carried out with MNase (New England BioLabs) at 4 U MNase per 200 μl of reaction buffer at 25°C for the indicated period of time. The reaction was terminated by adding an equal volume of 2 × TNE-SK buffer (20 mM Tris-HCl, pH 7.4, 0.2 M NaCl, 2 mM EDTA and 2% SDS) with freshly added proteinase K (0.2 mg/ml). The samples were then incubated overnight at 37°C, and genomic DNA was purified and separated by agarose gel electrophoresis.

Real-time polymerase chain reaction analysis

The extraction of total RNA and reverse-transcription of complementary DNA were performed as previously described (30). Quantitative real-time PCR (qRT-PCR) was performed in a 20 μl reaction mixture using SYBR qPCR master mix (Tiangen) and the 7500 real-time PCR system (Applied Biosystems). The primers used for real-time PCR were as follows:

Gene	Forward	Reverse
<i>Tbr2</i>	CCGGGACAACACTACGATTCCA	ACCTCCAGGGACAATCTGATG
<i>Tuj1</i>	CCAGTGC GGCAACCAGATAGG	AAAGGCGCCAGACCGAACACT
<i>Cend1</i>	AGTGGCTGCAGAAAGGAGATT	CACAACCTCTCGGCAGTCAA
<i>NeuroD1</i>	CTCAGCATCAATGGCAACTTCT	GACTCGCTCATGATGCGGAATGC
	C	C
<i>H2A.z</i>	GGCCGTATTCATCGACACCT	GACGAGGGGTGATACGCTTT
<i>H2A.v</i>	CTGGGCTCCAGTTTCTGTG	AGGTACTCCAGAATTGCGGC
<i>Nkx2-4</i>	GCTACTCGTCAATCCAGG	CAGGTACTTCTGCTGTTGAA
<i>Actin</i>	AGGTCATCACTATTGGCAACGA	CACCTCATGATGGAATTGAATG
		TAGTT

qRT-PCR primers ChIP-qPCR primers

Target (Nkx2-4) site	Forward	Reverse
-2k	GCAGTTCCAGCATAAGTGAC C	CATACTGTGGGACAAAATGC CAG
-1k	AGAGAGCTGTCGTTTTAACCC TG	GTTTGTAAATGGATCTTTTTG GTGGT
-300 bp	GCTCCGTTATCTGGAAGGG	TCCAGTGCCAGGTTTACGAC

Apoptosis assay

Apoptotic cells were detected by TUNEL assay using the In Situ Cell Death Detection Kit-TMR Red (Roche) according to the protocol.

ChIP-qPCR and ChIP-sequencing

ChIP analysis was performed essentially as previously described (34,35). Briefly, E13 neural progenitor cells were crosslinked with 1% formaldehyde solution (50 mM, HEPES-KOH, pH 7.5, 100 mM NaCl, 1 mM EDTA, 0.5 mM EGTA and 1% formaldehyde) for 10 min at room temperature, and the reaction was quenched with glycine. After washing twice with ice-cold PBS, cells were resuspended in lysis buffer 1 (50 mM HEPES-KOH, pH 7.5, 140 mM NaCl, 1 mM EDTA, 10% glycerol, 0.5% NP-40, 0.25% Triton X-100, 1 × protease inhibitors) for 10 min at 4°C. Nuclei were isolated at 4000 rpm for 5 min at 4°C and resuspended in lysis buffer 2 (10 mM Tris-HCl, pH 8.0, 200 mM NaCl, 1 mM EDTA, 0.5 mM EGTA, 1 × protease inhibitors) and then rocked gently at room temperature for 10 min. Nuclei were sonicated in lysis buffer 3 (1% SDS, 10 mM EDTA, 50 mM Tris-HCl pH 8.1, 1 × Protease Inhibitor) using a Scientz-IID sonicator. Chromatin was immunoprecipitated overnight at 4°C with 50 μl Protein A beads (Dynabeads, Invitrogen) pre-coupled with 2 μg appropriate antibodies. Beads were washed three times with low-salt buffer (0.1% SDS, 1% Triton X-100, 2 mM EDTA, 150 mM NaCl, Tris-HCl, pH 8.1) and three times with high-salt buffer (0.1% SDS, 1% Triton X-100, 2 mM EDTA, 500 mM NaCl, Tris-HCl, pH 8.1). After reverse crosslinking was performed, DNA was eluted and purified using a DNA purification kit (Tiangen) and subjected to qRT-PCR on the ABI 7500 real-time PCR system (Applied Biosystems). ChIP-seq was performed essentially as described above. Samples were sequenced using the Illumina HiSeq™ 4000. The raw reads were mapped to the mouse reference genome (mm9) by the Clean data processing pipeline, allowing up to two mismatches. The genome ChIP-seq profiles were generated using MACS2 with only

unique mapped reads. The data for H2A.z has been deposited in NCBI's GEO and are accessible through GEO Series accession number GSE99348. The ChIP-seq raw data for H3K36me3 in E13 WT and *H2A.z^{CKO}* forebrain has been deposited in NCBI's GEO and are accessible through GEO Series accession number GSE106679.

Open field test

Male mice (8–9 weeks old) were gently placed into an open field arena (40 cm width × 40 cm length × 40 cm height) and allowed to explore freely for 5 min (36). The locomotor activity and time spent in the center and margin areas were monitored and analyzed by the Topscan behavioral analysis software (Clever Sys Inc., Reston, VA, USA). Testing occurred in a dimly lit room maintained at 30–40 lux.

Elevated-plus maze

Testing was performed as previously described (37). Mice were placed in the center of the maze and allowed to explore freely for 5 minutes. The elevated-plus maze has two open arms and two closed arms (each arm 40 cm × 9.5 cm; height of closed arms 9.5 cm). The maze stood 40 cm above the ground. The percentage of time mice spent in the open and closed arms was analyzed.

Forced swim test

Testing was performed as previously described (38). Briefly, the forced swim test was carried out in a 20-cm diameter and 35 cm high cylindrical container filled with water (20 cm high) at 25°C. Behavior over a 6-min period was recorded, and only the last 4 minutes were analyzed.

Fear conditioning

Testing was performed as previously described (39). Briefly, mice were placed in a fear conditioning apparatus chamber for 2 min to habituate them to the environment and trained with three repeats of a 28.5 s, 80 dB tone that co-terminated with a 0.6 mA, 1.5 s shock (US). Mice were then returned to their home cage. One day after conditioning, the mice underwent both contextual fear conditioning and cued tests. For the contextual fear conditioning test, the mice were exposed to the original contextual chamber for 5 min. After 2 h of the contextual test, the cued test was performed. Mice were exposed to a novel context and permitted to explore freely for 2 min, and freezing behavior in response to a CS sound lasting 60 s was scored by the SMART v2.5.21 software.

Y-Maze

Spontaneous alternation testing was carried out in the Y-maze test as previously described (40,41). The procedure consisted of two phases: the training phase and the testing phase. During the training phase, mice were allowed to explore two arms of the Y-maze with the third arm (the 'novel arm') blocked for 5 min. After a 15-min interval, the testing phase was performed, and mice were allowed to explore all three arms freely for 5 min. The sequence of arm choices was recorded by the Topscan behavioral analysis software.

Three-chamber social interaction test

The three-chamber apparatus consisted of a transparent acrylic box with three equally sized chambers (25 cm × 25 cm), which could be closed or opened with a 5-cm door between each dividing wall. The three-chamber social test for sociability and social recognition/preference was performed as previously described with minor modifications (37). Briefly, the social interaction behavior test comprised two parts: a habituation session and two trial sessions. For the habituation session, two cylindrical wire cages were placed in the left and right chambers, and the test mice were habituated to all three chambers of the apparatus for 5 minutes.

After the habituation period, a wire cage containing an unfamiliar mouse (Stranger 1) was placed on one side of the chamber, and an empty mesh cage was placed on the other side. The test mice were moved into the middle chamber and allowed to freely explore all three chambers for 5 min. Following this period, a novel stranger mouse (Stranger 2) was placed in the empty cage, and again the test animal was left to explore for another 5 min. The time spent in each chamber, the total duration of active contacts such as sniffing and close huddling, and the trajectory of the test mice were calculated using the Topscan behavioral analysis software.

Statistical analysis

All data represent means ± S.E.M. Statistical comparisons in this study were performed using the unpaired *t*-test, Kolmogorov–Smirnov test and one-way ANOVA. Differences were considered significant with a *P* value of *P* < 0.05 (*), *P* < 0.01(**) or *P* < 0.001(***). n.s., not significant. All statistical analyses were performed using Excel 2016 (Microsoft) or GraphPad Prism 6.0.

RESULTS

H2A.z is expressed in the developing brain

To explore the role of H2A.z in brain development, we first detected the expression pattern of H2A.z in the brain from E11 to P1. Western blotting showed that H2A.z was highly expressed at E11 and gradually decreased with the progression of corticogenesis (Figure 1A), indicating that H2A.z might have important functions in brain development. H2A.z and H2A.v, differing by only three amino acids at the protein level, are encoded by distinct nucleotide sequences (42). We further performed quantitative RT-PCR (qRT-PCR) using *H2A.z* and *H2A.v* specific primers. The temporal expression pattern of *H2A.v* in the developing cortex was similar to that of *H2A.z* (Supplementary Figure S1A), with a reduction in expression throughout early development. Immunostaining revealed that H2A.z was ubiquitously expressed in the developing cortex and dominantly localized to the nucleus in the VZ/SVZ at E13 (Figure 1B and C). In addition, we found that H2A.z was not only co-labeled with Nestin, Sox2 and Pax6 but also co-expressed with Tuj1 (Figure 1D; Supplementary Figure S1B and C), indicating the expression of H2A.z in neural progenitor cells and neurons in the developmental cortex. To confirm the expression of H2A.z *in vitro*, neural progenitor cells isolated

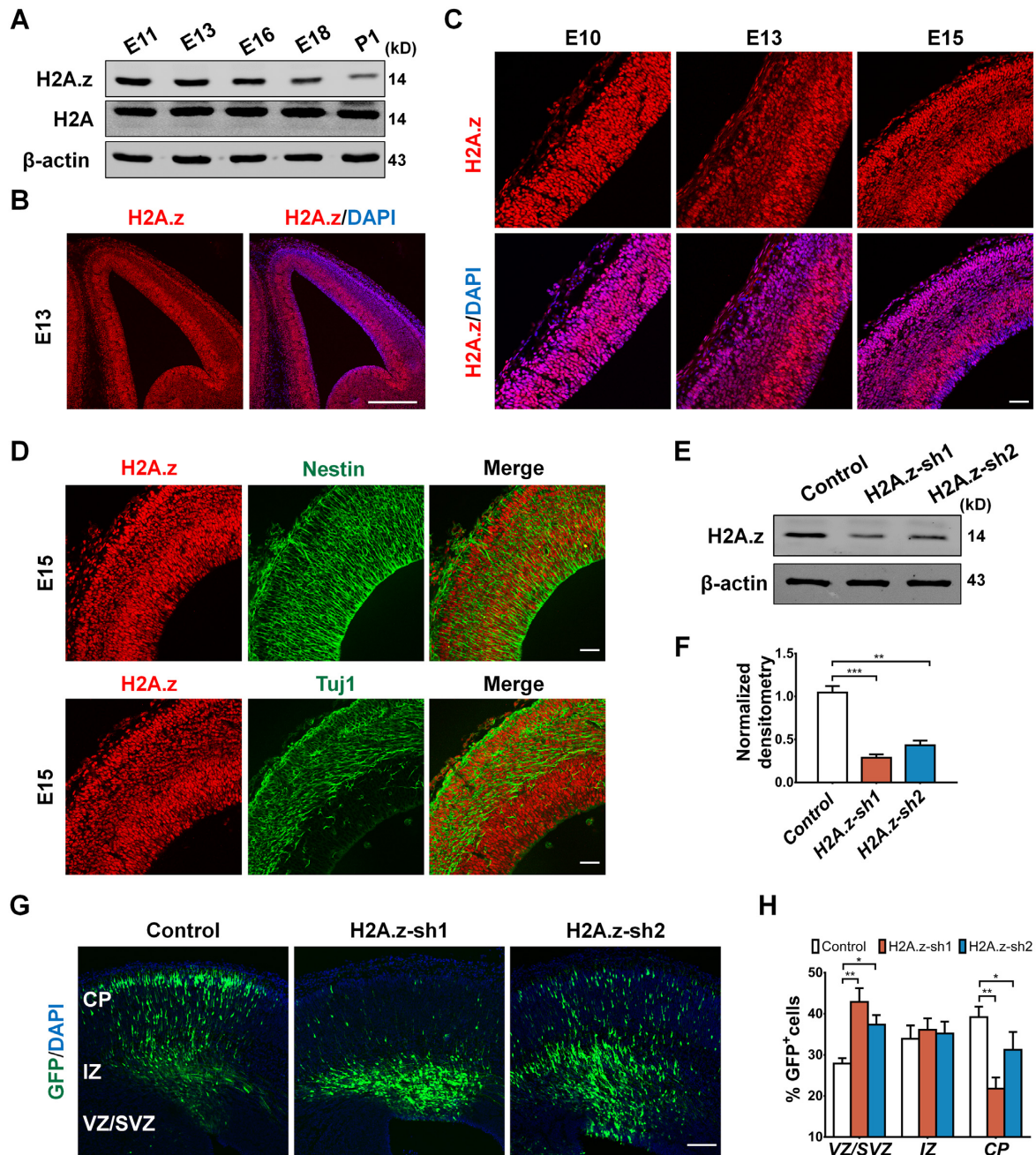


Figure 1. H2A.z is expressed in the embryonic cerebral cortex. (A) Western blot analysis of H2A.z in the development of the cerebral cortex. Brains in different developmental stages were isolated and lysed for western blot analysis with the antibodies indicated. (B) An overview of E13 brain sections labeled for H2A.z and DAPI. (C) Images of brain sections of the developing cerebral cortex labeled for H2A.z and DAPI. (D) H2A.z is abundantly expressed in Nestin positive neural progenitors and co labeled with Tuj1-positive neurons in the embryonic cortex. The E15 brain sections were immunostained with anti-H2A.z and anti-Nestin or anti-Tuj1 antibodies. (E) Western blot analysis reveals that the expression of H2A.z is effectively suppressed by *H2A.z*-shRNAs in primary neural progenitors. (F) Graph shows that the amount of H2A.z is obviously decreased in *H2A.z*-shRNA lentivirus-infected primary neural progenitors. $n = 5$ for all samples. (G) Electroporation of *H2A.z*-shRNAs results in abnormal cell distribution in the developing neocortex. The electroporation was performed at E13, and the mouse was sacrificed at E16. (H) Graph shows the percentage of GFP-positive cells distributed in the VZ/SVZ, IZ and CP. $n = 5$ for all samples. Representative images from at least three independent experiments. Error bars represent means \pm S.E.M.; Two-tailed unpaired *t*-test, $P < 0.05$ (*), $P < 0.01$ (**) or $P < 0.001$ (***). n.s., not significant. CP, cortical plate; IZ, intermediate zone; VZ/SVZ, ventricular/subventricular zone. Scale bar represents 100 μ m (B); 20 μ m (C and D); 50 μ m (G).

from E12 brains were used for analysis. Immunostaining assays revealed that H2A.z was also expressed in dissociated neural progenitors. In line with the findings *in vivo*, the immunoreactivity of H2A.z was weaker in Tuj1-positive cells (Supplementary Figure S1C).

To identify the functions of H2A.z in embryonic neurogenesis, two shRNAs were used to knock down the expression of H2A.z. Western blotting showed that endogenous H2A.z was obviously reduced in *H2A.z*-shRNA lentivirus-infected primary neural progenitor cells (Figure 1E and F). Next, two *H2A.z*-shRNAs and the control were delivered to E13 brains through *in utero* electroporation, and the brains were harvested at E16. H2A.z was also decreased in shRNA-electroporated cells *in vivo* (Supplementary Figure S1D and E). Simultaneously, exogenous Flag-H2A.z was also efficiently reduced in *H2A.z*-shRNA-transfected N2a cells (Supplementary Figure S1F). Upon *H2A.z* knockdown, we observed a consistent overall increase in the number of GFP⁺ cells in the VZ/SVZ where neural progenitors reside, suggesting a profound increase in proliferation (Figure 1G and H). Consistently, the number of GFP⁺ cells in the cortical plate (CP) was obviously decreased (Figure 1G and H). Taken together, these results suggest that H2A.z is required for cortical neurogenesis.

H2A.z regulates brain neural progenitor cell proliferation

Given that more GFP⁺ cells were observed in the VZ/SVZ, where neural progenitors are enriched, we next examined whether the increase in GFP⁺ cells was due to enhanced neural progenitor proliferation. We next used pH3 to label mitotically active cells and observed an increase in mitotic activity in *H2A.z*-knockdown embryos (Supplementary Figure S2A and B). We further labeled the cycling neural progenitors with BrdU for 2h before analysis. The brains immunostaining with antibody against BrdU showed that *H2A.z* shRNAs caused an increase in BrdU incorporation in the GFP⁺ cell population (Supplementary Figure S2C and D). To further explore the role of H2A.z in brain development, *H2A.z*^{fl/fl} mice were crossed with *Nestin-Cre* mice to generate *H2A.z* conditional knockout (*H2A.z*^{CKO}) mice. Immunostaining showed that the expression of H2A.z was depleted in E13 *H2A.z*^{CKO} brains (Supplementary Figure S2E). Of note, there was no significant difference in the number of apoptotic cells between *H2A.z*^{fl/fl} and *H2A.z*^{CKO} mice (Supplementary Figure S2F and G), indicating that the abnormal cell distribution is not caused by cell death. In addition to this, we observed that *H2A.z* knockout caused an increase in the number of pH3-positive cells in the rostral, central, and caudal areas of E16 mouse cortices (Figure 2A and B), indicating that mitotic activity was increased when H2A.z was absent. Consistently, the immunolabeling of BrdU on coronal sections from *H2A.z*^{fl/fl} and *H2A.z*^{CKO} embryos showed that more BrdU-incorporating cells were detected in *H2A.z*^{CKO} embryos (Figure 2C and D), suggesting that progenitor cells in S phase were also increased when *H2A.z* was ablated.

Radial glial cells (RGs) and intermediate progenitors (IPs) are two major types of progenitors in the VZ/SVZ (43). Our *in vivo* data raised the question of whether *H2A.z* knockout affected the lineage progression from VZ to SVZ

progenitors. For this purpose, we compared the proportions of Pax6⁺ cells and Tbr2⁺ cells in the *H2A.z*^{fl/fl} and *H2A.z*^{CKO} embryos. Although the number of Pax6⁺ cells was not significantly affected (Supplementary Figure S2H and I), Tbr2⁺ cells were increased in the VZ/SVZ regions of *H2A.z* knockout mice (Figure 2E). To clarify whether the increase in Tbr2⁺ cells is due to the proliferation of IPs, we labeled the proliferated IPs by injecting BrdU for 2h before analysis. As expected, the amplification of IPs, which were Tbr2⁺BrdU⁺, was increased, while the proliferation of RGs showed no obvious alteration after *H2A.z* was deleted (Figure 2F; Supplementary Figure S2J). Consistently, the expression of Tbr2 was increased at the protein and mRNA levels, while no significant variation was found in Pax6 when *H2A.z* was lost (Supplementary Figure S3A–C). To test whether the promoted proliferation of *H2A.z* knockout NPCs was cell autonomous or influenced by external cues, we isolated primary NPCs from E12 forebrain in order to form neurospheres in culture. Compared with *H2A.z*^{fl/fl}, the neurosphere size formed from *H2A.z*^{CKO} NPCs was obviously increased (Figure 2G and H). Then, we electroporated GFP plasmid into the embryonic brains of *H2A.z*^{fl/fl} mice and *H2A.z*^{CKO} mice at E13, and we harvested the brains at E16. Compared to *H2A.z*^{fl/fl} mice, *H2A.z*^{CKO} mice also showed an abnormal distribution of GFP-positive cells (Figure 2I and J), which was similar to the results of *H2A.z* knockdown. Quantification confirmed that a higher proportion of GFP-positive cells resided in the VZ/SVZ in *H2A.z*^{CKO} mice, suggesting that the loss of *H2A.z* promoted the ability of neural progenitor cells to maintain their proliferative potential.

In the following experiments, we electroporated the plasmid of *H2A.z* overexpression into WT or *H2A.z*^{CKO} brains (Supplementary Figure S3D). First, we found that overexpression of *H2A.z* caused decreased in the percentage of GFP-positive cells in the VZ/SVZ compared to controls. This was accompanied by a concomitant increase proportion of GFP-positive cells in the cortical plate and decreased BrdU incorporation (Supplementary Figure S3E–G). Overexpression of *H2A.z* in *H2A.z*-knockout embryos are able to normalize the distribution of GFP⁺ cells to control levels as well as restore levels of BrdU incorporation (Supplementary Figure S3E–G). Hence, these data demonstrated an early intrinsic control of H2A.z on the proliferation of NPCs.

Loss of H2A.z expression impairs neurogenesis

To examine if the decreased proportion of GFP-positive cells in the cortical plate leads to decreased neuronal differentiation, we stained electroporated brains with antibody against Tuj1 (Figure 3A). Quantification of GFP⁺Tuj1⁺ cells revealed that the knockdown of *H2A.z* led to a decrease in the percentage of GFP⁺Tuj1⁺ cells, indicating that *H2A.z* knockdown caused a reduction in neuronal differentiation in the developing mouse cortex (Figure 3B). Interestingly, the mRNA level of *H2A.v* remained unaltered upon loss of *H2A.z* in E13 *H2A.z*^{CKO} cortex (Supplementary Figure S4A). To confirm these variant-specific functions, we further performed *in utero* electroporation with sequence-specific shRNAs for *H2A.z* and *H2A.v* individu-

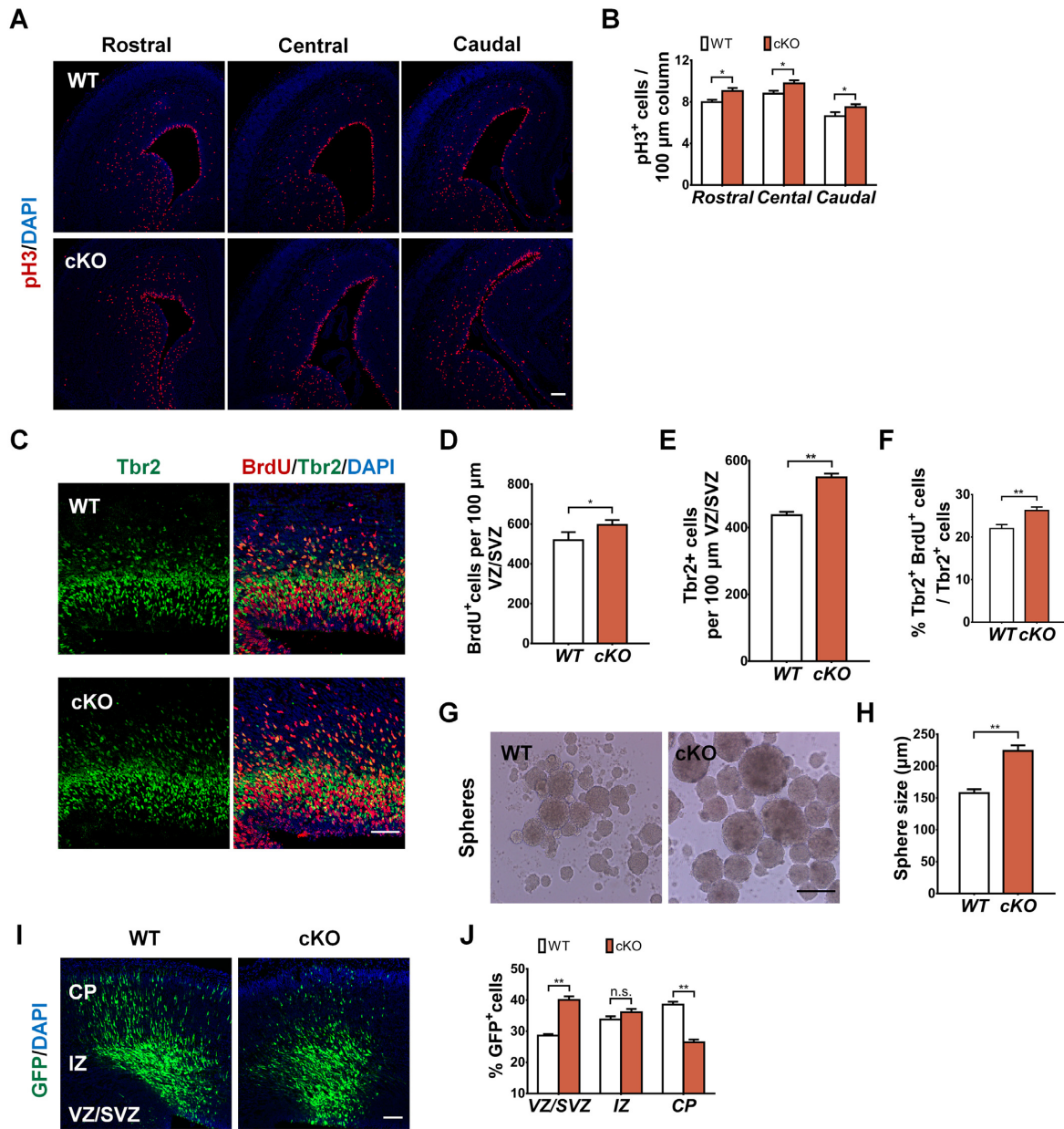


Figure 2. *H2A.z* regulates the proliferation of NPCs during brain development. (A) Brain sections of *H2A.z^{fl/fl}* mice and *H2A.z^{cKO}* mice at E16 were immunostained with mitotic marker pH3 and DAPI. (B) Statistics of pH3-positive cells in rostral, central, and caudal areas of the cortex. $n = 5$ for all samples. (C) Representative images of E16 coronal brain sections were immunostained for Tbr2 and BrdU. BrdU was injected intraperitoneally to pregnant mice at E16 for 2 h of pulse labeling. (D) Statistic of BrdU-positive cells per 100 μm^2 surface of VZ/SVZ. $n = 7$ for all samples. (E) Statistics of Tbr2-positive cells per 100 μm^2 surface of VZ/SVZ. $n = 6$ for all samples. (F) Percentage of Tbr2⁺BrdU⁺ cells among all Tbr2⁺ cells. $n = 7$ for all samples. (G) Neural progenitor cells isolated from *H2A.z^{cKO}* mice form larger neurospheres. Primary neural progenitors were dissociated from E12 *H2A.z^{cKO}* or *H2A.z^{fl/fl}* mice and seeded at low density (50 cells/ml), then cultured in proliferated medium (suspension culture) for 3 days. (H) Statistic of the diameters of neurospheres. $n = 8-9$ for all samples. (I) Abnormal cell distribution is observed in *H2A.z* ablated neocortex. The GFP plasmid was electroporated into E13 mouse brains of *H2A.z^{fl/fl}* mice and *H2A.z^{cKO}* mice, and the mice were sacrificed at E16. (J) Graphs of the percentage of GFP-positive cells in the VZ/SVZ, IZ and CP. $n = 8-10$ for all samples. Representative images from at least three independent experiments. *H2A.z^{fl/fl}*, WT; *H2A.z^{cKO}*, cKO. CP, cortical plate; IZ, intermediate zone; VZ/SVZ, ventricular/subventricular zone. Error bars represent means \pm S.E.M.; Two-tailed unpaired t-test, $P < 0.05$ (*), $P < 0.01$ (**) or $P < 0.001$ (***), n.s., not significant. Scale bar represents 15 μm (A); 20 μm (C); 80 μm (G); 50 μm (I).

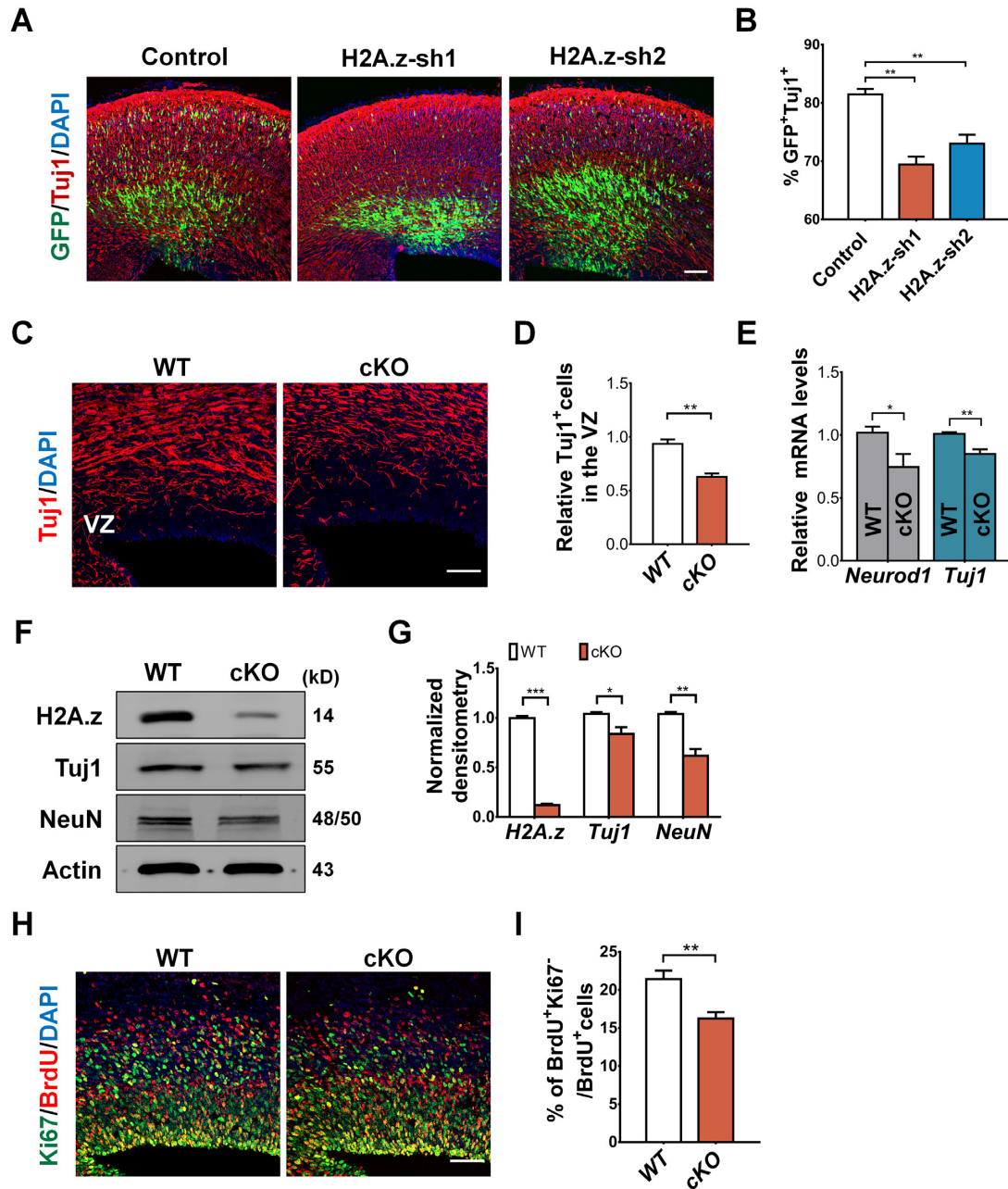


Figure 3. H2A.z regulates the differentiation of NPCs. (A) The number of neurons is decreased in *H2A.z*-shRNA-electroporated brains. Neurons were labeled with anti-Tuj1 in E16 brain sections. (B) Percentage of Tuj1⁺GFP⁺ cells among GFP⁺ cells. *n* = 4 for all samples. (C) Coronal brain slices of E16 *H2A.z^{fl/fl}* and *H2A.z^{cKO}* mice were immunostained using anti-Tuj1. (D) Relative Tuj1⁺ cells in the VZ of *H2A.z^{fl/fl}* and *H2A.z^{cKO}* mice. *n* = 8 for all samples. (E) The mRNA level of *NeuroD1* and *Tuj1* is decreased in *H2A.z*-deleted neurospheres. E12 primary neural progenitor cells (NPCs) were isolated from *H2A.z^{cKO}* and *H2A.z^{fl/fl}* mice, and cultured in proliferation medium (suspension culture) for 3 days, and then collected the neurospheres for further analysis (E and F). *Actin* mRNA served as an internal control. *n* = 4 for all samples. (F) Western blot analysis reveals that the expression levels of the neuron markers Tuj1 and NeuN are downregulated in *H2A.z*-loss neurospheres. (G) Statistics of the normalized density of H2A.z, Tuj1 and NeuN. *n* = 6 for all samples. (H) Cell cycle exit is decreased in *H2A.z^{cKO}* mice. E16 brain sections were stained with anti-BrdU and anti-Ki67. *H2A.z^{fl/fl}* mice and *H2A.z^{cKO}* mice were administered BrdU (100 mg/kg) for 24 h and were euthanized at E16. (I) Percentage of cell cycle exit (BrdU⁺Ki67⁻/Ki67⁺) in *H2A.z^{fl/fl}* or *H2A.z^{cKO}* mice. *n* = 6 for all samples. Representative images from at least three independent experiments. *H2A.z^{fl/fl}*, WT; *H2A.z^{cKO}*, cKO. VZ, ventricular zone. Error bars represent means ± S.E.M.; two-tailed unpaired *t*-test, *P* < 0.05 (*), *P* < 0.01(**) or *P* < 0.001(***)). Scale bar represents 50 μm (A); 20 μm (C and H).

ally or combinationally at E13 and analyzed brains at E16. It is worth noting that loss of *H2A.z*, but not *H2A.v*, disrupts the distribution of GFP-positive cells in the developing cortex (Supplementary Figure S4B–D). Besides the distribution change, we noticed that knockdown of *H2A.z* and *H2A.v* combination did not additively increase the percentage of cells positive for neuronal marker Tuj1 (Supplementary Figure S4E). In addition to this, immunofluorescence staining of Tuj1 revealed a decrease in the spontaneous neuronal differentiation of Pax6⁺ neural progenitors in *H2A.z*-knockout embryonic brains at E16 (Figure 3C and D; Supplementary Figure S4F and G). Moreover, we performed RT-PCR and western blotting analysis of neurospheres derived from the cortex. This approach ensured that our analysis included differentiation capacity of NPCs only in a cell-autonomous manner. We quantified the mRNA or protein levels of neuronal differentiation-related markers such as NeuroD1, Tuj1 and NeuN in *H2A.z*-deleted neural progenitors and found that the loss of *H2A.z* expression led to a decrease in neuronal differentiation (Figure 3E–G), in accordance with our Tuj1 immunocytochemistry results. To test this directly, we injected BrdU into pregnant mice for 24 h prior to brain analysis at E16, followed by immunofluorescence staining of BrdU and Ki67. Using this analysis, we found that the percentage of cells exiting the cell cycle (the percentage of BrdU+Ki67⁻/BrdU+Ki67⁺ cells) was reduced when *H2A.z* was deleted (Figure 3H and I), indicating that the increase in cell proliferation was accompanied by decreased cell cycle exit.

The reduced differentiation of progenitors prompted us to examine the neuronal cell-type specification. Staining with layer-specific markers at P0 revealed that *H2A.z* knockout did not affect the positioning of neurons within the cortical plate (Supplementary Figure S5A, D and G). In *H2A.z*^{CKO} neocortex at P0, we found an increase in the number of Cux1⁺ neurons (layers II–III) (Supplementary Figure S5A and B), along with a concomitant reduction in Tbr1⁺ cells (layer VI) (Supplementary Figure S5G and H). To examine whether progenitor cell cycle kinetics altered the timing of neurogenesis we pulse-labeled progenitors with BrdU at E13 then analyzed with layer-specific markers and BrdU at P0. We observed a reduction of the production of Cux1⁺BrdU⁺ neurons (Supplementary Figure S5C) and an increase in the number of Tbr1⁺BrdU⁺ cells in the *H2A.z*^{CKO} cortex (Supplementary Figure S5I). In addition, the numbers of Ctip2⁺ (layer V) neurons and the proportion of Ctip2⁺ BrdU⁺ neurons were not altered between WT and *H2A.z*CKO mice (Supplementary Figure S5D–F).

***H2A.z* deletion results in abnormal neuronal morphology**

To test whether the loss of *H2A.z* affects the morphology of neurons during brain development, primary NPCs isolated from GFP plasmid-electroporated brains were differentiated for 4 or 6 days *in vitro*. The results showed that not only the total length of the dendrites but also the number of primary dendrites was reduced in *H2A.z*-deleted neurons after four days of differentiation (Figure 4A–C). Similar results were observed in *H2A.z*-suppressed neurons (Supplementary Figure S6A and B). After 6 days of differentiation,

the reductions in dendritic length and branching number in *H2A.z*-loss neurons were still observed (Figure 4D and E). Related to this, we performed *in utero* electroporation in E13 WT or *H2A.z*^{CKO} embryos with GFP plasmid and analyzed brains at P0 or P5 (Figure 4F; Supplementary Figure S6C). We found that the *H2A.z*-loss neurons after their migration also exhibited abnormal dendritic morphology (Figure 4F and G; Supplementary Figure S6C–F). Furthermore, we found that abnormal GFP⁺ cell distribution upon loss of *H2A.z* is obvious in early brain development (Supplementary Figure S7A–D). Nevertheless, to confirm a cell-intrinsic function of *H2A.z* and rule out the possible contribution of other cell types in the brain affecting the dendritic development, we performed *in utero* electroporation in E13 embryos with shRNAs for *H2A.z* and *H2A.v* individually or combinationally and analyzed at P17 (Supplementary Figure S7E). It is worth noting that loss of *H2A.z*, but not *H2A.v*, caused a dramatic reduction in branching (Supplementary Figure S7F). Knockdown of *H2A.z* and *H2A.v* combinationally did not additively cause an obvious reduction in branch number (Supplementary Figure S7F), further demonstrating *H2A.v* has no additive effect on dendritic complexity. Altogether, these results demonstrate that *H2A.z* is essential for dendritic growth.

Loss of *H2A.z* in developing brain results in behavioral abnormalities in adult mice

The *H2A.z*^{CKO} mice can survive to adulthood and show a reduced bodyweight in comparison to the control mice (Supplementary Figure S8A–D). Furthermore, the brain weights of P0 *H2A.z*^{CKO} mice were indistinguishable from those of control mice (Supplementary Figure S8E and F). However, significant reductions in brain weights (by ~15%) were observed in adult brain (Supplementary Figure S8G and H). To test whether the deletion of *H2A.z* during cortical development results in behavioral deficits in adult mice, *H2A.z*^{CKO} mice and their littermate *H2A.z*^{fl/fl} mice were first subjected to the open field test. Compared with the controls, *H2A.z*^{CKO} mice spent less time in the central area, although they showed no apparent difference in motility (Figure 5A–C). These results suggested that exploratory behavior was reduced in *H2A.z*^{CKO} mice. Next, we employed the elevated-plus maze to measure whether the *H2A.z*^{CKO} mice showed anxiety-like behavior. Compared with the control, *H2A.z*^{CKO} mice spent less time in the open arms, while they spent more time in the closed arms of the maze (Figure 5D–F). These data further supported that the loss of *H2A.z* resulted in reduced exploratory behavior in adult mice. To test whether *H2A.z*^{CKO} mice were abnormal in social interaction, three-chamber social arena assays were performed (Supplementary Figure S9A–D). In these assays, *H2A.z*^{fl/fl} mice spent more time in the chamber where a novel stranger mouse (Stranger 2) was placed in the cage, whereas *H2A.z*^{CKO} mice did not display an apparent preference (Figure 5G). Furthermore, *H2A.z*^{fl/fl} mice tended to interact with the mouse in the novel cage, while the *H2A.z*^{CKO} mice were inactive in terms of contact with the novel mouse (Figure 5H). These data suggest that the loss of *H2A.z* results in deficiencies in social interaction. Next, the forced swim test was used to detect whether *H2A.z*^{CKO} mice had

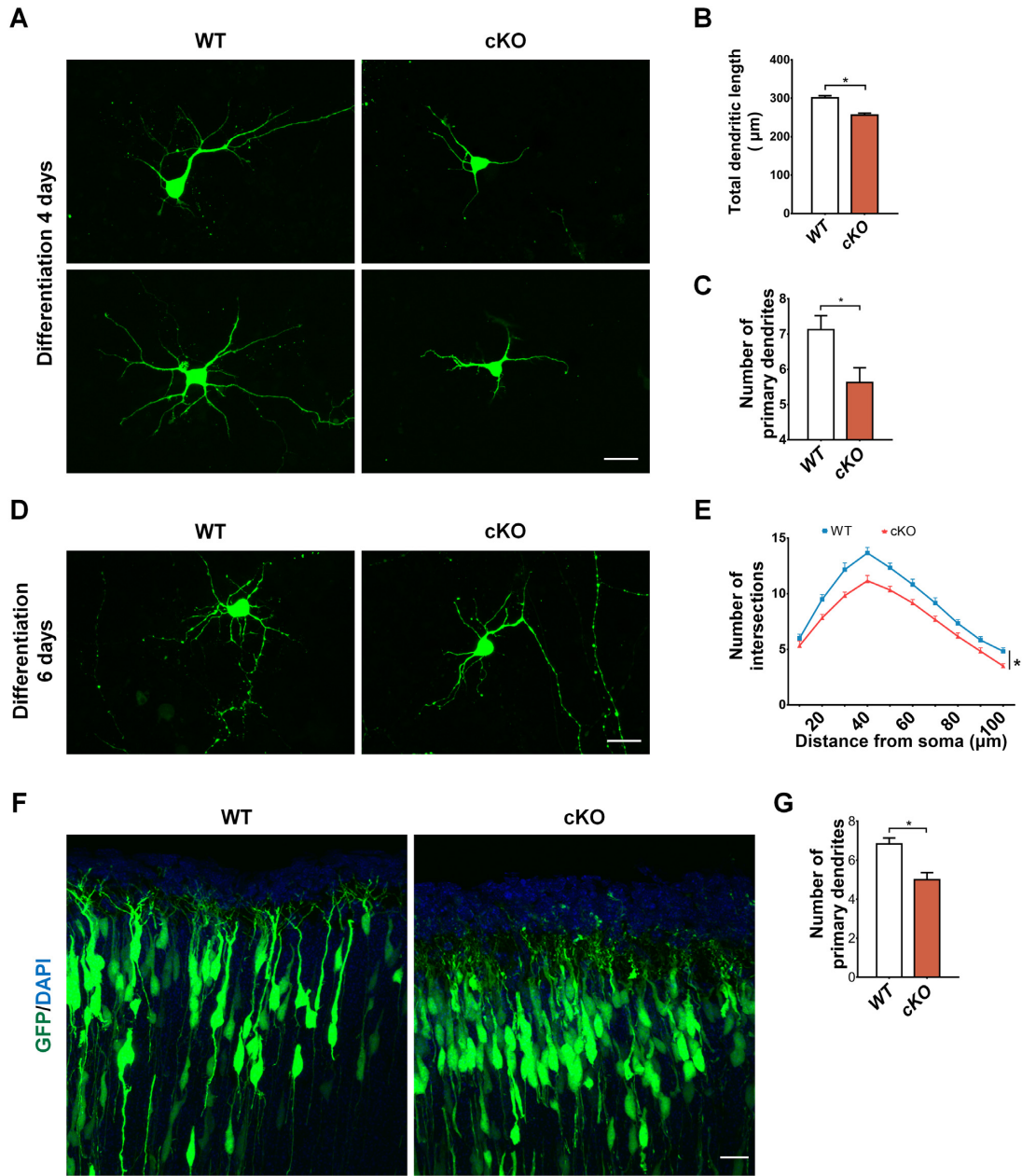


Figure 4. The loss of *H2A.z* results in abnormal morphology of neurons. (A) Representative images of neurons after 4 days of culture *in vitro*. GFP-expressing plasmid was electroporated into the E13 cerebral cortices of *H2A.z^{fl/fl}* or *H2A.z^{cKO}* mice to mark neural progenitor cells. After 24 h, the GFP-positive cells were isolated and cultured in differentiation medium for 4 days. (B) Graph shows that the total dendritic length of neurons is decreased when *H2A.z* is deleted. *n* = 8 cells from three samples. (C) Statistics show that the number of primary dendrites is reduced upon *H2A.z* deletion. *n* = 8 cells from three samples. (D) Images of neurons cultured in differentiation medium for 6 days. (E) Sholl graphs of dendrites of neurons electroporated with GFP alone in *H2A.z^{fl/fl}* or *H2A.z^{cKO}* mice. The GFP-positive cells were isolated and cultured in differentiation medium for 6 days. *H2A.z^{fl/fl}*, *n* = 6 cells; *H2A.z^{cKO}*, *n* = 6 cells. (F) High-magnification confocal images of upper layer show that *H2A.z* knockout results in abnormally branched processes compared to the control. GFP plasmid was electroporated into the *H2A.z^{fl/fl}* or *H2A.z^{cKO}* embryonic brain at E13 and harvested at P0. (G) Quantification of dendritic numbers in *H2A.z^{fl/fl}* and *H2A.z^{cKO}* cortices. *n* = 6 for all samples. Representative images from at least three independent experiments. *H2A.z^{fl/fl}*, WT; *H2A.z^{cKO}*, cKO. Error bars represent means ± S.E.M., Kolmogorov–Smirnov test or two-tailed unpaired *t*-test, *P* < 0.05 (*), *P* < 0.01 (**). Scale bar represents 15 μm (A and D); 10 μm (F).

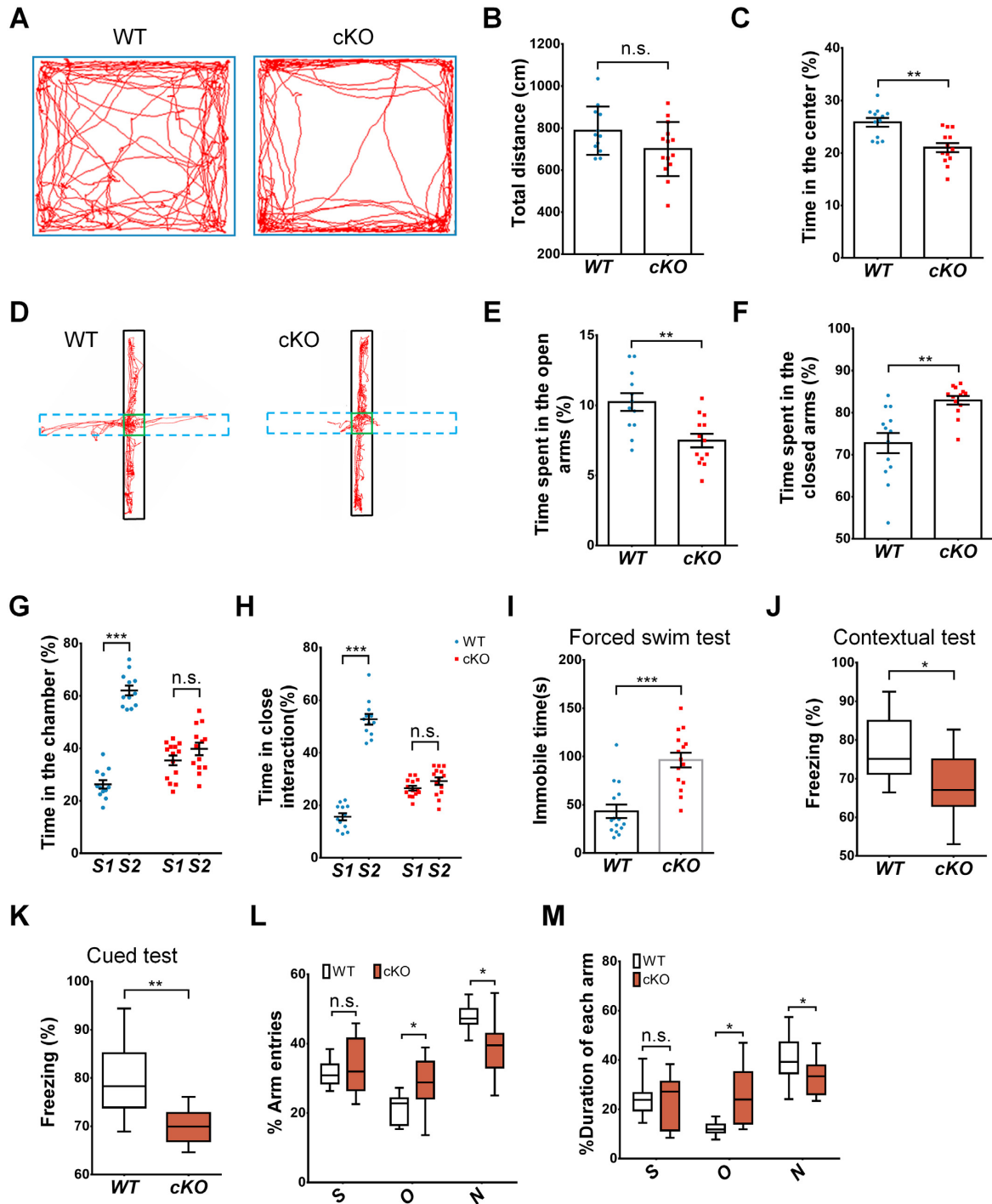


Figure 5. The loss of *H2A.z* results in behavioral deficits. (A) Representative tracing pathway of *H2A.z^{fl/fl}* and *H2A.z^{cKO}* mice in the open field test. (B) The total traveling distance was not different between *H2A.z^{fl/fl}* and *H2A.z^{cKO}* mice. (C) Time spent in the center is reduced in *H2A.z^{cKO}* mice. (D) Representative tracing pathway of *H2A.z^{fl/fl}* and *H2A.z^{cKO}* mice in the elevated-plus maze test. (E) *H2A.z^{cKO}* mice spent less time in the open arms. (F) *H2A.z^{cKO}* mice spent more time in the closed arms. (G) Social interaction behavior is impaired in *H2A.z*-null mice. *H2A.z^{cKO}* mice spent similar time in the chamber with the stranger 1 or stranger 2 mouse, while *H2A.z^{fl/fl}* mice spent more time in the chamber with stranger 2 than with the stranger 1 mouse. (H) Close social interaction is affected by *H2A.z* deletion. *H2A.z^{cKO}* mice did not spend more time in close interaction with stranger 2 than with stranger 1. (I) The immobile time of *H2A.z^{cKO}* mice was more than that of *H2A.z^{fl/fl}* mice during the forced swim test. (J) The percentage of freezing in *H2A.z^{cKO}* mice was less than in *H2A.z^{fl/fl}* mice, although they were explored in the same background. (K) Freezing response was also reduced in *H2A.z^{cKO}* mice in the cued test. (L) Compared with *H2A.z^{fl/fl}* mice, the entries of *H2A.z^{cKO}* mice into new arms were decreased, while the entries into old arms were increased. (M) Compared with *H2A.z^{fl/fl}* mice, *H2A.z^{cKO}* mice spent less time in the new arms and more time in the old arms. All mice were male, 8–10 weeks old. *H2A.z^{fl/fl}*, WT, $n = 11–14$; *H2A.z^{cKO}*, cKO, $n = 9–16$. Error bars represent means \pm S.E.M.; one-way ANOVA, $P < 0.05$ (*), $P < 0.01$ (**) or $P < 0.001$ (***). n.s., not significant. Analysis was performed by an experimenter blinded to experimental conditions.

depressive-like states. Compared with the control, the immobile time of *H2A.z^{CKO}* mice was increased, indicating that *H2A.z^{CKO}* mice were prone to depression (Figure 5I). To evaluate the learning and memory of *H2A.z^{CKO}* mice, fear conditioning tests and Y-maze tests were performed. The results revealed that the freezing percentage of the *H2A.z^{CKO}* mice was decreased compared with the control mice, indicating that the loss of *H2A.z* impaired the associative memory (Figure 5J and K). The Y-maze test showed that the *H2A.z^{CKO}* mice were less prone to enter new arms and spent less time in the new arms, indicating that the working memory was affected (Figure 5L and M; Supplementary Figure S9E). Taken together, the results from this range of behavior tests indicate that *H2A.z^{CKO}* mice exhibit behavioral deficits in exploratory activity, social behavior and spatial learning and memory. In addition, *H2A.z^{CKO}* mice are prone to anxiety and depression.

H2A.z regulates neurogenesis by targeting Nkx2-4

To gain deeper insight into how H2A.z regulates embryonic neurogenesis, RNA sequencing (RNA-seq) was performed to analyze the genome-wide changes resulting from *H2A.z* deletion at E13 (Supplementary Figure S10A). Gene ontology analysis showed that the downregulated genes were enriched in terms related to transcription and cortex development, such as regulation of transcription, cerebellar cortex formation, forebrain development, and cerebellum development (Figure 6A). Upregulated genes showed a significant enrichment of terms involved in the negative regulation of cell differentiation, neuron migration, and cognition (Figure 6B). These results reflected the importance of H2A.z in cortical development. Because the genomic localization of H2A.z might reveal its essential role during early neurogenesis, ChIP-seq was performed on developing mouse E13 forebrain as previously described (35). As expected, H2A.z was prone to bind the promoter (32.4%) and the intergenic regions (32.1%) (Figure 6C). The analysis of biological processes of H2A.z-bound genes indicate H2A.z play roles in pathways relating to cell cycle, DNA replication and chromatin disassembly (Figure 6D). In addition, we examined the overlap between H2A.z ChIP-seq peaks with differentially expressed genes in mRNA-seq data of *H2A.z* deletion and subdivided GO terms for H2A.z-bound genes into the 2 classes: upregulated or downregulated group upon deletion of *H2A.z* (Figure 6E). Downregulated genes enriched in H2A.z ChIP-seq peaks were involved in processes relating to microtubule cytoskeleton organization, dendritic spine morphogenesis and growth (Figure 6F). Upregulated genes are involved in regulation of glucose metabolic process, reproductive process, stem cell population maintenance and mitotic division (Figure 6G). We next investigated how *H2A.z* deletion affected the molecular program controlling cortical neurogenesis. We focused on studying Nkx2-4, because it showed the reduction in E13 H2A.z-deficient forebrain (Figure 6H; Supplementary Figure S10B–D; Supplementary Table S1). Furthermore, it was reported Nkx2-4 may be involved in the regionalization of the forebrain and may affect embryonic neurogenesis (44).

A key aspect of the regulation of gene expression during neurogenesis occurs at the level of chromatin states (8). We consider that the coordination of transcription with histone modifications is critical for gene regulation. We first detected the methylations of histone upon *H2A.z* knock-out. Notably, the level of H3K36me3 was reduced, while no obvious variation was detected in the levels of H3K27me3, H3K9me3, and H3K4me3 in the E13 brain, suggesting that H2A.z incorporation can affect global H3K36me3 modification patterns (Supplementary Figure S10E and F). In accordance with previous observations (34), H3K36me3 ChIP-seq signals were distributed in both the body and the promoter of genes (Supplementary Figure S10G). We further evaluated the patterns of H3K36me3 enrichment in the E13 *H2A.z^{CKO}* forebrain and found that H3K36me3 is decreased throughout the whole genome (Figure 6I, Supplementary Figure S10H). Furthermore, we found the amount of H3K36me3 in the gene body and the promoter regions of Nkx2-4 was decreased in response to H2A.z loss (Supplementary Figure S10I). These data indicate that H2A.z mediates transcriptional initiation of *Nkx2-4*.

To confirm whether H2A.z regulates embryonic neurogenesis through targeting *Nkx2-4*, we further investigate the role of Nkx2-4 in cortical development. Using a specific antibody against Nkx2-4, we examined Nkx2-4 protein expression in the developing forebrain (E12–E18). Nkx2-4 was localized to the nucleus in neural progenitors in the VZ/SVZ and newborn neurons in the CP. Furthermore, we found Nkx2-4 protein was broadly expressed in Tuj1⁺ neurons, Tbr2⁺ IPs and Sox2⁺ progenitors (Supplementary Figure S11A–C). Similarly, the GFP⁺ cells in the VZ/SVZ were increased, while the number of GFP⁺ cells in the cortical plate was obviously reduced when the expression of Nkx2-4 was downregulated (Supplementary Figure S11D–F). Immunostaining of pH3 showed that more pH3 signals were observed in the VZ/SVZ regions in the *Nkx2-4*-suppressed cortex (Supplementary Figure S11G). Consistently with the results for H2A.z, the percentage of Tuj1-positive cells was also decreased in *Nkx2-4* knockdown samples (Supplementary Figure S11H and I).

Considering that *Nkx2-4* is an important gene downstream of H2A.z, we next detected whether the overexpression of Nkx2-4 could rescue the developmental deficiency caused by *H2A.z* downregulation. For this purpose, *H2A.z*- or *Nkx2-4*-overexpression plasmids were co-electroporated with *H2A.z* shRNA into E13 brains, which were harvested at E16. We found that co-expression of *Nkx2-4* with *H2A.z*-sh1 restored the distribution of GFP⁺ cells, the percentage of GFP⁺ Tbr2⁺ cells and mitotic activity, as well as the percentage of GFP⁺ Tuj1⁺ cells (Supplementary Figure S12A–H). To determine whether forced Nkx2-4 expression could also rescue the dendritic abnormalities associated with H2A.z loss-of-function, we performed in utero electroporation at E13 with control, H2A.z-sh1 or co-expressed either control empty vector or Nkx2-4 overexpression constructs, and analyzed brains at P17. The reduction in branching of upper layer neurons was partially rescued upon Nkx2-4 co-expression (Supplementary Figure S12I and J). Thus, *Nkx2-4* is an important downstream gene of H2A.z during embryonic neurogenesis.

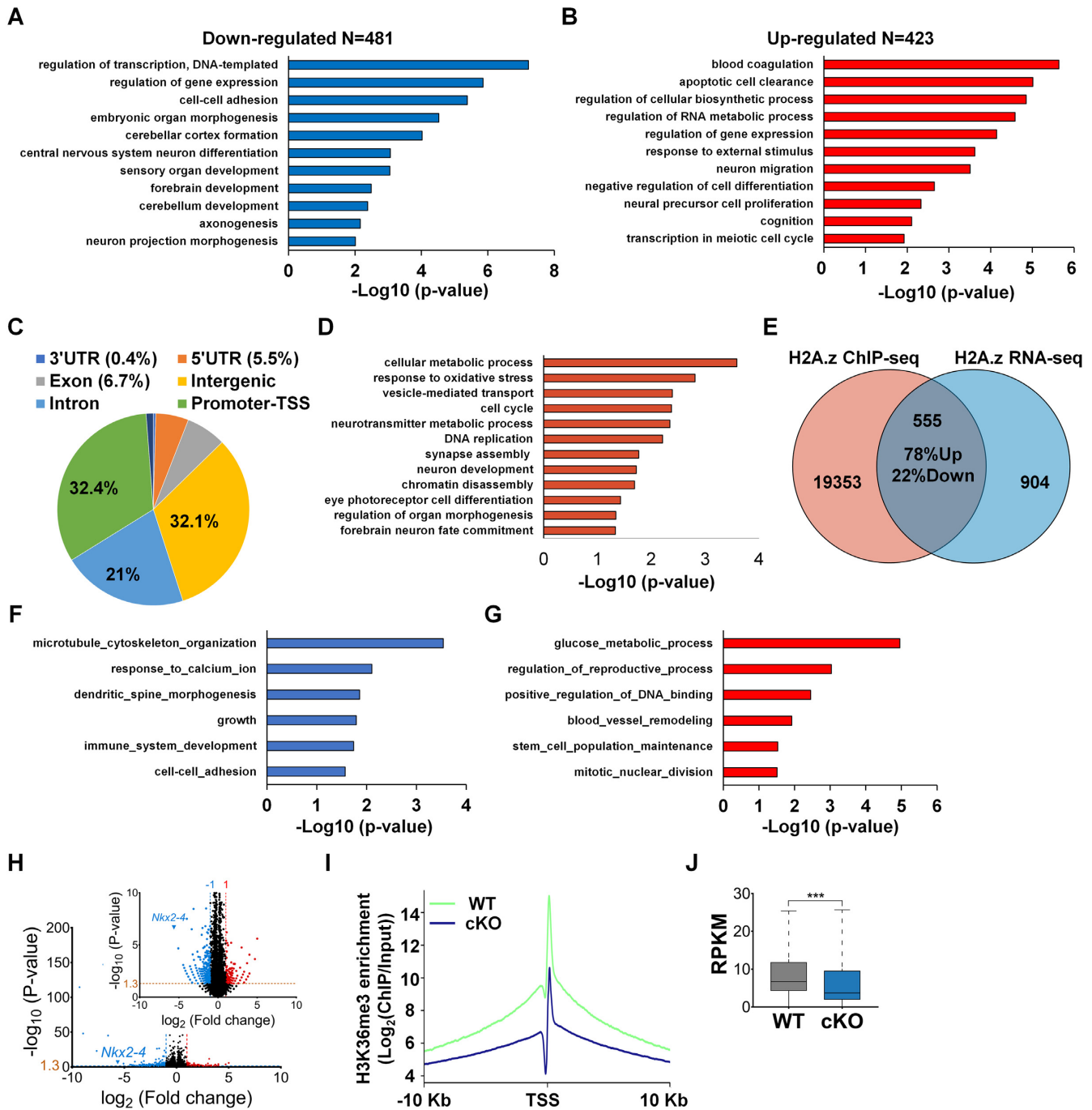


Figure 6. H2A.z regulates neurogenesis by targeting Nkx2-4. (A) GO analysis for downregulated genes from E13 forebrain RNA-seq data sets in *H2A.z*-loss mice. (B) Analysis of gene ontology of biological functions for upregulated genes in *H2A.z*-depleted E13 forebrain. (C) Genome-wide distribution of H2A.z occupancies in E13 forebrain. (D) GO analyses of H2A.z binding genes. (E) Venn diagram showing the overlap between H2A.z bound genes by ChIP-seq with differentially expressed genes following *H2A.z* knockout (RNA-seq). (F) GO analyses for H2A.z-bound genes which are downregulated upon deletion of *H2A.z*. (G) GO analyses for H2A.z-bound genes which are upregulated upon deletion of *H2A.z*. (H) Volcano plots illustrate differentially expressed genes. Red dots are upregulated genes, and green dots are downregulated genes compared to the control. *Nkx2-4* is one of the significantly differentially expressed genes. (I) H3K36me3 occupancy for all genes in E13 WT and *H2A.z^{cKO}* forebrain. (J) RPKM values for all genes in E13 WT and *H2A.z^{cKO}* forebrain.

H2A.z and Setd2-mediated H3K36me3 modification regulate Nkx2-4

Having shown that H2A.z mediated transcriptional initiation of Nkx2-4 during early neurogenesis, we set out to address the mechanism by which H2A.z regulates this pathway. Setd2 is a histone methyltransferase that specifically trimethylates Lys-36 of histone H3 (Supplementary Figure S13A and B) (45). We further detected the relationship between H2A.z and Setd2. A co-immunoprecipitation (co-IP) experiment showed that H2A.z could interact with Setd2 (Figure 7A-C and Supplementary Figure S13C). Higher H3K36me3 levels were also detected in the overexpression of both H2A.z and Setd2 than in H2A.z or Setd2 overexpression alone, indicating that H2A.z promotes the trimethylation of Setd2 on Lys-36 of histone H3 (Figure 7B and C). Western blotting showed that H3K36me3 levels and Nkx2-4 expression were reduced when both H2A.z and Setd2 were knocked down (Figure 7D). Consistently, the expression of Nkx2-4 and the level of H3K36me3 were both increased when H2A.z and Setd2 were overexpressed, while no obvious variation was found when H2A.z was overexpressed, suggesting that H2A.z and Setd2 coordinately increase H3K36me3 levels and Nkx2-4 expression (Figure 7E). Simultaneously, H2A.z overexpression could rescue the reduced H3K36me3 and Nkx2-4 levels caused by H2A.z knockdown, while H2A could not, indicating that the regulatory effect of H2A.z on H3K36me3 modification and Nkx2-4 expression is specific (Figure 7F). In addition, the regulatory effect of H2A.z on neurogenesis is also specific (Supplementary Figure S13D and E). Consistently with the ChIP-seq results, the binding enrichment of H2A.z in the *Nkx2-4* promoter is higher in 300 bp upstream of TSS (Supplementary Figure S13F). In addition, the chromatin accessibility is reduced upon H2A.z deletion (Supplementary Figure S13G). To show that the regulatory effect of H2A.z on the *Nkx2-4* promoter is via interaction with Setd2, the binding enrichment of H2A.z and Setd2 on the *Nkx2-4* promoter was detected by ChIP experiments. When H2A.z was knocked down, the binding enrichment of Setd2 in the *Nkx2-4* promoter region was reduced (Figure 7G). When Setd2 was knocked down, the accumulation of H2A.z in *Nkx2-4* promoter region was not altered (Figure 7H). In contrast, the accumulation of H2A.z in *Nkx2-4* promoter region was increased when Setd2 was overexpression (Figure 7I). Furthermore, the accumulation of H3K36me3 in the *Nkx2-4* promoter region was abolished in both H2A.z-silenced and Setd2-OE NPCs (Figure 7J). These results indicate that H2A.z plays essential roles in recruiting Setd2 onto the *Nkx2-4* promoter.

DISCUSSION

Embryonic neurogenesis is a critical process for brain development, which is regulated in a spatially and temporally restricted manner (2). Dysregulation of any of these steps might result in abnormal brain functions, thereby contributing to the occurrence of neurodevelopmental disorders (6,46). H2A.z, an evolutionarily conserved histone variant, not only plays essential roles in chromatin organization and stability but also is critical for the epigenetic regulation of gene expression (23). Previous reports show that

H2A.z has important functions in key biological processes (23,25). However, the role of H2A.z in embryonic neurogenesis remains largely unknown. Here, we take advantage of H2A.z conditional knockout mice to explore the functions of H2A.z in neural progenitor proliferation and differentiation, neuronal morphology, and mouse behavior, as well as the underlying mechanisms. We find that H2A.z interacts with Setd2 to increase the H3K36me3 levels of the *Nkx2-4* promoter, thereby increasing the expression of Nkx2-4. Taken together, the epigenetic regulation of H2A.z is essential for brain development.

We find that H2A.z is expressed in the embryonic cerebral cortex and gradually decreased with brain development. Our finding demonstrates that knockdown or knockout of H2A.z promotes the proliferation of NPCs and inhibits neuronal differentiation. Current available data indicate that H2A.z acts as a critical factor that mediates the activation of differentiation-associated genes (18,47). The reason for these differences may be that H2A.z regulates cell proliferation in a cell type-specific manner (48,49).

Neuronal dendritic arborization is acquired soon after neurons have entered their destined cortical layer in the brain (50). Our study demonstrates that H2A.z is crucial for dendritic morphology. We show that the dendritic morphology of neurons is impacted by the embryonic removal of H2A.z. Dendritic morphogenesis is crucial for the functional integration of neurons from neural progenitors and the establishment of neuronal connectivity (51). Abnormal dendrite morphogenesis leads to neuronal dysfunctions associated with neurodevelopmental disorders such as schizophrenia and autism (52-54). Furthermore, using H2A.z^{CKO} mice as a model, we demonstrate that in addition to the neuronal differentiation defects, the loss of H2A.z causes behavioral defects resembling the characteristics of patients with autism and schizophrenia. Interestingly, the H2A.z gene has been suggested as a risk factor for schizophrenia. Thus, our study provides further evidence for the recognition of H2A.z as a risk gene for neurodevelopmental disorders. Earlier studies have implicated H2A.z as a negative regulator of the consolidation of recent and remote memory (55). In our study, freezing responses were found to be reduced in H2A.z^{CKO} mice. This discrepancy could be due to differences in the timing and level of H2A.z suppression. In addition to this, we cannot rule out the possibility of changes of other type of cells such as astrocytes and oligodendrocytes in H2A.z^{CKO} brain. It is fascinating to consider how loss of H2A.z function only in astrocytes or oligodendrocytes might directly or indirectly contribute to the altered behavior.

Next, we examined dysregulated genes in H2A.z^{CKO} via the RNA-sequencing analysis of E13 brain samples. We find that *Nkx2-4* RNA expression is reduced in H2A.z^{CKO} relative to H2A.z^{fl/fl}. The homeodomain (HD) protein Nkx2-4 is a member of the Nkx2 family, but less is known about the specification of *Nkx2-4* in the development of the brain. Herein, we show that the depletion of *Nkx2-4* promotes the proliferation and inhibits the differentiation of neural progenitors. Further, increasing Nkx2-4 levels promotes the differentiation of neural progenitors and rescues the impaired neurogenesis resulting from H2A.z knockdown.

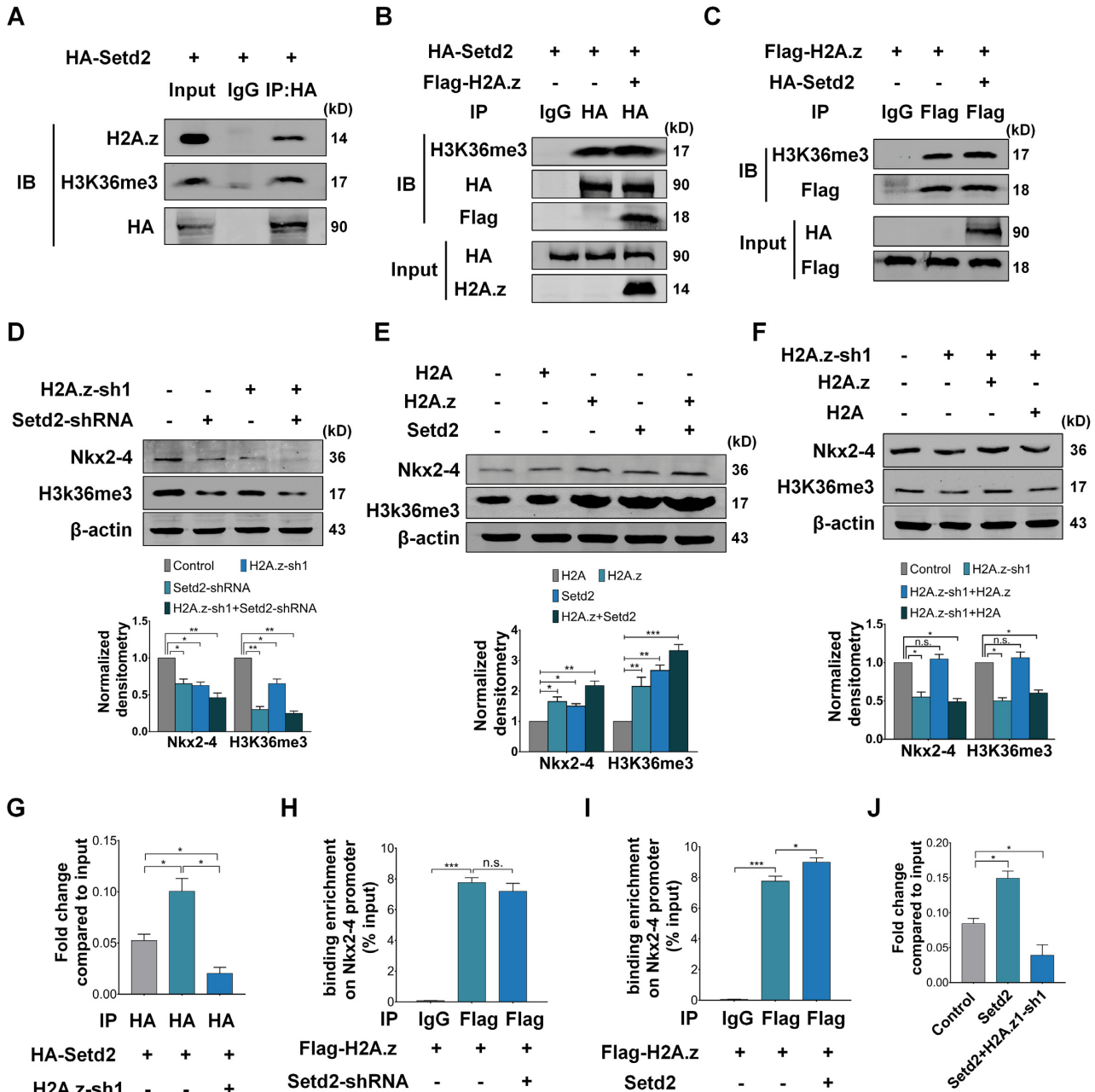


Figure 7. H2A.z and Setd2-mediated H3K36me3 on Nkx2-4 promoter regulate the expression of Nkx2-4. (A) The interaction between H2A.z and Setd2 is verified by co-immunoprecipitation experiments. HA-Setd2-expressing plasmids were transfected into N2A cells. Three days later, the transfected cells were subjected to immunoprecipitation using HA beads. Bound proteins were detected by western blotting with the antibodies indicated. (B) H2A.z promotes Setd2-mediated H3K36me3 modification. HA-Setd2 plasmids were co-transfected with Flag-H2A.z or control into N2A cells. The cell lysates were immunoprecipitated with anti-HA, and bound proteins were detected by western blotting with the antibodies indicated. (C) Higher H3K36me3 levels were pulled down in both the H2A.z and Setd2 overexpression groups. Flag-H2A.z plasmids were co-transfected with HA-Setd2 or control into N2A cells. The cell lysates were immunoprecipitated with anti-Flag and blotted with the antibodies indicated. (D) The levels of H3K36me3 and Nkx2-4 are decreased when both *H2A.z* and *Setd2* are silenced. Primary neural progenitors were infected with lentivirus indicated (D, E and F). Three days later, the cell lysates were analyzed by western blotting with the antibodies indicated. Graph below depicts quantification for Nkx2-4 and H3K36me3, normalized to actin. (E) Higher levels of Nkx2-4 and H3K36me3 are detected when H2A.z and Setd2 are overexpressed, while no obvious increase is investigated when H2A is overexpressed. Graph below depicts quantification for Nkx2-4 and H3K36me3, normalized to actin. (F) Overexpression of H2A.z, but not H2A, can rescue the downregulation of Nkx2-4 and H3K36me3 caused by *H2A.z*-sh1. Graph below depicts quantification for Nkx2-4 and H3K36me3, normalized to actin. (G) ChIP in primary neural progenitors overexpressing Setd2 with or without *H2A.z*-sh1, as indicated, performed with antibodies indicated. (H) ChIP in primary neural progenitors overexpressing H2A.z with or without Setd2-shRNA, as indicated, performed with antibodies indicated. (I) ChIP in primary neural progenitors overexpressing H2A.z with or without Setd2, as indicated, performed with antibodies indicated. (J) ChIP analysis of enrichment of H3K36me3 on promoters of *Nkx2-4* in primary neural progenitors infected with control, Setd2 or Setd2 together with *H2A.z*-sh1 lentivirus. A total of 5% of input was loaded for western blotting. Representative images from at least three independent experiments. ChIP enrichment is expressed as percentage of input. $n = 3-4$ for all samples. Error bars represent means \pm S.E.M.; two-tailed unpaired *t*-test, $P < 0.05$ (*), $P < 0.01$ (**) or $P < 0.001$ (***). n.s., not significant.

Analogous to other members (56), our findings suggest that *Nkx2–4* has key roles in brain development.

Previously, the genome-wide binding properties and activity of H2A.z in the developing brain were unknown. It is reported that H2A.z is deposited at enhancers and promoters that exhibit bivalent signatures with both activating (H3K4me3; H3K36me3) and repressive (H3K27me3; H3K9me3) histone modifications (23). Indeed, our data show the promoter enrichment of H2A.z with both up- and downregulation of gene expression in *H2A.z^{cKO}*, suggesting that H2A.z binding shows context-dependent activity. The transcriptional changes in *Nkx2–4* might be due to direct regulation by H2A.z or might be mediated indirectly via the functions of H2A.z-regulated genes. We then examine the relationship between H2A.z binding and chromatin state. In this regard, we compared histone modifications results from *H2A.z^{fl/fl}* and *H2A.z* conditional knockout at E13 to reveal H2A.z as an epigenetic regulator. The level of H3K36me3 was reduced when *H2A.z* was depressed. Setd2 (SET-domain containing 2), also known as KMT3A and HYPB, is recognized as a histone methyltransferase responsible for the trimethylation of histone H3 at Lys 36 (H3K36me3) (45). It is now well established that H3K36me3 is an epigenetic marker associated with gene transcription (57). Local recruitment of Setd2 by H2A.z could explain the changes in H3K36me3 associated with *Nkx2–4* in *H2A.z^{cKO}*. We found that the loss of H2A.z impairs the recruitment of Setd2 and is correlated with reduced levels of H3K36me3 and *Nkx2–4* protein. Furthermore, H3K36me3 is decreased throughout the whole genome, as well as at the transcription start site of *Nkx2–4* in response to H2A.z loss. Thus, H2A.z appears to potentiate chromatin accessibility by modulating nucleosome occupancy at regulatory regions. Consistent with these observations, knockout of *H2A.z* results in decreased chromatin accessibility by micrococcal nuclease (MNase). In contrast to H2A.z, H2A cannot rescue the deficiency in embryonic neurogenesis caused by *H2A.z*-shRNAs. In addition, H2A.z, but not H2A, can rescue the downregulation of H3K36me3 and *Nkx2–4* resulting from *H2A.z* knockdown. These results indicate that the regulatory effect of H2A.z on embryonic neurogenesis is unique and cannot be replaced by H2A. Here, we elucidate the molecular functions of H2A.z by integrating its genome-wide binding, regulation of gene expression, and epigenetic state to delineate the mechanisms by which H2A.z instructs cortical development.

Taken together, our results emphasize the essential role of the epigenetic regulation of H2A.z in embryonic neurogenesis and highlight the important functions of H2A.z in brain development. We find that H2A.z regulates the recruitment of Setd2 to promote the H3K36me3 levels of the *Nkx2–4* promoter, thereby increasing the expression of *Nkx2–4*, which ultimately controls neuron production and the expansion of the cerebral cortex. Furthermore, the behavioral abnormalities in H2A.z-null mice provide a possible explanation for the deficits found in patients with schizophrenia (27). In summary, our findings reveal the role of H2A.z in embryonic neurogenesis and dendrite morphogenesis, and how H2A.z loss may lead to various developmental defects and brain disorders (Supplementary Figure S14).

DATA AVAILABILITY

Data have been deposited in NCBI's GEO and are accessible through GEO Series accession number GSE99347 (RNA-sequencing analysis), GSE99348 (H2A.z), GSE106679 (H3K36me3 in E13 WT and H2A.zKO forebrain).

SUPPLEMENTARY DATA

Supplementary Data are available at NAR Online.

ACKNOWLEDGEMENTS

We thank Wenlong Xia, Qingli Liang and Libo Su for their valuable comments. We are grateful to Shiwen Li and Xili Zhu for help with confocal imaging. We also thank Hua Qin and Baoguo Li for advice about behavioral analyses.

Author contributions: T.S. initiated, performed, and analyzed the experiments. Y.W., X.L. and D.Z. did several of the experiments. F.J. wrote the manuscript. J.J. supervised the project and acquired the funding support. All authors read and approved the final manuscript.

FUNDING

National Science Foundation of China [31730033, 31621004]; National Key Basic Research Program of China [2015CB964500, 2014CB964903, 2014CB964602]; K.C. Wong Education Foundation; Strategic Priority Research Program [XDA16020602]. Funding for open access charge: National Science Foundation of China [31730033, 31621004]; National Key Basic Research Program of China [2015CB964500, 2014CB964903, 2014CB964602]; K.C. Wong Education Foundation; Strategic Priority Research Program [XDA16020602].

Conflict of interest statement. None declared.

REFERENCES

1. Monuki, E.S. and Walsh, C.A. (2001) Mechanisms of cerebral cortical patterning in mice and humans. *Nat. Neurosci.*, **4** Suppl, 1199–1206.
2. Noctor, S.C., Martinez-Cerdeno, V., Ivic, L. and Kriegstein, A.R. (2004) Cortical neurons arise in symmetric and asymmetric division zones and migrate through specific phases. *Nat. Neurosci.*, **7**, 136–144.
3. Evsyukova, I., Plestant, C. and Anton, E.S. (2013) Integrative mechanisms of oriented neuronal migration in the developing brain. *Annu. Rev. Cell Dev. Biol.*, **29**, 299–353.
4. Mao, Y., Ge, X., Frank, C.L., Madison, J.M., Koehler, A.N., Doud, M.K., Tassa, C., Berry, E.M., Soda, T., Singh, K.K. *et al.* (2009) Disrupted in schizophrenia 1 regulates neuronal progenitor proliferation via modulation of GSK3beta/beta-catenin signaling. *Cell*, **136**, 1017–1031.
5. Sugathan, A., Biagioli, M., Golzio, C., Erdin, S., Blumenthal, I., Manavalan, P., Ragavendran, A., Brand, H., Lucente, D., Miles, J. *et al.* (2014) CHD8 regulates neurodevelopmental pathways associated with autism spectrum disorder in neural progenitors. *Proc. Natl. Acad. Sci. U.S.A.*, **111**, E4468–E4477.
6. Ernst, C. (2016) Proliferation and differentiation deficits are a major convergence point for neurodevelopmental disorders. *Trends Neurosci.*, **39**, 290–299.
7. Hahn, M.A., Qiu, R., Wu, X., Li, A.X., Zhang, H., Wang, J., Jui, J., Jin, S.G., Jiang, Y., Pfeifer, G.P. *et al.* (2013) Dynamics of 5-hydroxymethylcytosine and chromatin marks in Mammalian neurogenesis. *Cell Rep.*, **3**, 291–300.

8. Yao, B., Christian, K.M., He, C., Jin, P., Ming, G.L. and Song, H. (2016) Epigenetic mechanisms in neurogenesis. *Nat. Rev. Neurosci.*, **17**, 537–549.
9. Shen, T.J., Ji, F. and Jiao, J.W. (2015) Epigenetics: major regulators of embryonic neurogenesis. *Sci. Bull.*, **60**, 1734–1743.
10. Nord, A.S., Pattabiraman, K., Visel, A. and Rubenstein, J.L. (2015) Genomic perspectives of transcriptional regulation in forebrain development. *Neuron*, **85**, 27–47.
11. Albert, M., Kalebic, N., Florio, M., Lakshmanaperumal, N., Haffner, C., Brandl, H., Henry, I. and Huttner, W.B. (2017) Epigenome profiling and editing of neocortical progenitor cells during development. *EMBO J.*, **36**, 2642–2658.
12. Yao, B. and Jin, P. (2014) Unlocking epigenetic codes in neurogenesis. *Genes Dev.*, **28**, 1253–1271.
13. Maze, I., Noh, K.M., Soshnev, A.A. and Allis, C.D. (2014) Every amino acid matters: essential contributions of histone variants to mammalian development and disease. *Nat. Rev. Genet.*, **15**, 259–271.
14. Henikoff, S., Furuyama, T. and Ahmad, K. (2004) Histone variants, nucleosome assembly and epigenetic inheritance. *Trends Genet. TIG*, **20**, 320–326.
15. Talbert, P.B. and Henikoff, S. (2010) Histone variants—ancient wrap artists of the epigenome. *Nat. Rev. Mol. Cell Biol.*, **11**, 264–275.
16. Papamichos-Chronakis, M., Watanabe, S., Rando, O.J. and Peterson, C.L. (2011) Global regulation of H2A.Z localization by the INO80 chromatin-remodeling enzyme is essential for genome integrity. *Cell*, **144**, 200–213.
17. Lashgari, A., Millau, J.F., Jacques, P.E. and Gaudreau, L. (2017) Global inhibition of transcription causes an increase in histone H2A.Z incorporation within gene bodies. *Nucleic Acids Res.*, **45**, 12715–12722.
18. Domaschensch, R., Kurscheid, S., Nekrasov, M., Han, S. and Tremethick, D.J. (2017) The histone variant H2A.Z is a master regulator of the epithelial-mesenchymal transition. *Cell Rep.*, **21**, 943–952.
19. Obri, A., Ouarrarhni, K., Papin, C., Diebold, M.L., Padmanabhan, K., Marek, M., Stoll, L., Roy, L., Reilly, P.T., Mak, T.W. *et al.* (2014) ANP32E is a histone chaperone that removes H2A.Z from chromatin. *Nature*, **505**, 648–653.
20. Lazorthes, S., Vallot, C., Briois, S., Aguirrebengoa, M., Thuret, J.Y., St Laurent, G., Rougeulle, C., Kapranov, P., Mann, C., Trouche, D. *et al.* (2015) A vlincRNA participates in senescence maintenance by relieving H2AZ-mediated repression at the INK4 locus. *Nat. Commun.*, **6**, 5971.
21. Wang, Y., Chen, X., Sheng, Y., Liu, Y. and Gao, S. (2017) N6-adenine DNA methylation is associated with the linker DNA of H2A.Z-containing well-positioned nucleosomes in *Pol II*-transcribed genes in *Tetrahymena*. *Nucleic Acids Res.*, **45**, 11594–11606.
22. Bargaje, R., Alam, M.P., Patowary, A., Sarkar, M., Ali, T., Gupta, S., Garg, M., Singh, M., Purkanti, R., Scaria, V. *et al.* (2012) Proximity of H2A.Z containing nucleosome to the transcription start site influences gene expression levels in the mammalian liver and brain. *Nucleic Acids Res.*, **40**, 8965–8978.
23. Hu, G., Cui, K., Northrup, D., Liu, C., Wang, C., Tang, Q., Ge, K., Levens, D., Crane-Robinson, C. and Zhao, K. (2013) H2A.Z facilitates access of active and repressive complexes to chromatin in embryonic stem cell self-renewal and differentiation. *Cell Stem Cell*, **12**, 180–192.
24. Faast, R., Thonglairoam, V., Schulz, T.C., Beall, J., Wells, J.R., Taylor, H., Matthaeci, K., Rathjen, P.D., Tremethick, D.J. and Lyons, I. (2001) Histone variant H2A.Z is required for early mammalian development. *Curr. Biol. CB*, **11**, 1183–1187.
25. Creighton, M.P., Markoulaki, S., Levine, S.S., Hanna, J., Lodato, M.A., Sha, K., Young, R.A., Jaenisch, R. and Boyer, L.A. (2008) H2AZ is enriched at polycomb complex target genes in ES cells and is necessary for lineage commitment. *Cell*, **135**, 649–661.
26. Wang, J., Qiao, M., He, Q., Shi, R., Loh, S.J., Stanton, L.W. and Wu, M. (2015) Pluripotency activity of nanog requires biochemical stabilization by variant histone protein H2A.Z. *Stem Cells*, **33**, 2126–2134.
27. Chang, M., Sun, L., Liu, X., Sun, W. and You, X. (2015) Association of common variants in H2AFZ gene with schizophrenia and cognitive function in patients with schizophrenia. *J. Hum. Genet.*, **60**, 619–624.
28. Kahn, R.S. and Sommer, I.E. (2015) The neurobiology and treatment of first-episode schizophrenia. *Mol. Psychiatry*, **20**, 84–97.
29. Pfister, S.X., Markkanen, E., Jiang, Y., Sarkar, S., Woodcock, M., Orlando, G., Mavrommati, I., Pai, C.C., Zalmas, L.P., Drobnitzky, N. *et al.* (2015) Inhibiting WEE1 selectively kills histone H3K36me3-deficient cancers by dNTP starvation. *Cancer Cell*, **28**, 557–568.
30. Ji, F., Shen, T., Zou, W. and Jiao, J. (2017) UCP2 regulates embryonic neurogenesis via ROS-mediated yap alternation in the developing neocortex. *Stem Cells*, **35**, 1479–1492.
31. Shen, T., Ji, F., Yuan, Z. and Jiao, J. (2015) CHD2 is required for embryonic neurogenesis in the developing cerebral cortex. *Stem Cells*, **33**, 1794–1806.
32. Xia, W. and Jiao, J. (2017) Histone variant H3.3 orchestrates neural stem cell differentiation in the developing brain. *Cell Death Differ.*, **24**, 1548–1563.
33. Xu, Z., Song, Z., Li, G., Tu, H., Liu, W., Liu, Y., Wang, P., Wang, Y., Cui, X., Liu, C. *et al.* (2016) H2B ubiquitination regulates meiotic recombination by promoting chromatin relaxation. *Nucleic Acids Res.*, **44**, 9681–9697.
34. Wen, H., Li, Y., Xi, Y., Jiang, S., Stratton, S., Peng, D., Tanaka, K., Ren, Y., Xia, Z., Wu, J. *et al.* (2014) ZMYND11 links histone H3.3K36me3 to transcription elongation and tumour suppression. *Nature*, **508**, 263–268.
35. Lee, T.I., Johnstone, S.E. and Young, R.A. (2006) Chromatin immunoprecipitation and microarray-based analysis of protein location. *Nat. Protoc.*, **1**, 729–748.
36. Dietrich, M.O., Zimmer, M.R., Bober, J. and Horvath, T.L. (2015) Hypothalamic *AgRP* neurons drive stereotypic behaviors beyond feeding. *Cell*, **160**, 1222–1232.
37. Orefice, L.L., Zimmerman, A.L., Chirila, A.M., Sleboda, S.J., Head, J.P. and Ginty, D.D. (2016) Peripheral mechanosensory neuron dysfunction underlies tactile and behavioral deficits in mouse models of ASDs. *Cell*, **166**, 299–313.
38. Libert, S., Pointer, K., Bell, E.L., Das, A., Cohen, D.E., Asara, J.M., Kapur, K., Bergmann, S., Preisig, M., Otowa, T. *et al.* (2011) SIRT1 activates MAO-A in the brain to mediate anxiety and exploratory drive. *Cell*, **147**, 1459–1472.
39. Xu, C., Krabbe, S., Grundemann, J., Botta, P., Fadok, J.P., Osakada, F., Saur, D., Grewe, B.F., Schnitzer, M.J., Callaway, E.M. *et al.* (2016) Distinct hippocampal pathways mediate dissociable roles of context in memory retrieval. *Cell*, **167**, 961–972 e916.
40. Ferreira, D.G., Temido-Ferreira, M., Miranda, H.V., Batalha, V.L., Coelho, J.E., Szego, E.M., Marques-Morgado, I., Vaz, S.H., Rhee, J.S., Schmitz, M. *et al.* (2017) alpha-synuclein interacts with PrPC to induce cognitive impairment through mGluR5 and NMDAR2B. *Nat. Neurosci.*, **20**, 1569–1579.
41. Belforte, J.E., Zsiris, V., Sklar, E.R., Jiang, Z., Yu, G., Li, Y., Quinlan, E.M. and Nakazawa, K. (2010) Postnatal NMDA receptor ablation in corticolimbic interneurons confers schizophrenia-like phenotypes. *Nat. Neurosci.*, **13**, 76–83.
42. Matsuda, R., Hori, T., Kitamura, H., Takeuchi, K., Fukagawa, T. and Harata, M. (2010) Identification and characterization of the two isoforms of the vertebrate H2A.Z histone variant. *Nucleic Acids Res.*, **38**, 4263–4273.
43. Stahl, R., Walcher, T., De Juan Romero, C., Pilz, G.A., Cappello, S., Irmeler, M., Sanz-Aguela, J.M., Beckers, J., Blum, R., Borrell, V. *et al.* (2013) *Trnp1* regulates expansion and folding of the mammalian cerebral cortex by control of radial glial fate. *Cell*, **153**, 535–549.
44. Sugahara, F., Pascual-Anaya, J., Oisi, Y., Kuraku, S., Aota, S., Adachi, N., Takagi, W., Hirai, T., Sato, N., Murakami, Y. *et al.* (2016) Evidence from cyclostomes for complex regionalization of the ancestral vertebrate brain. *Nature*, **531**, 97–100.
45. Chen, K., Liu, J., Liu, S., Xia, M., Zhang, X., Han, D., Jiang, Y., Wang, C. and Cao, X. (2017) Methyltransferase SETD2-mediated methylation of STAT1 is critical for interferon antiviral activity. *Cell*, **170**, 492–506 e414.
46. Birnbaum, R. and Weinberger, D.R. (2017) Genetic insights into the neurodevelopmental origins of schizophrenia. *Nat. Rev. Neurosci.*, **18**, 727–740.
47. Yang, S.S., Tan, J.L., Liu, D.S., Loreni, F., Peng, X., Yang, Q.Q., He, W.F., Yao, Z.H., Zhang, X.R., Dal Pra, I. *et al.* (2015) Eukaryotic initiation factor 6 modulates myofibroblast differentiation at transforming growth factor-beta1 transcription level via H2A.Z occupancy and Sp1 recruitment. *J. Cell Sci.*, **128**, 3977–3989.

48. Dalvai, M., Bellucci, L., Fleury, L., Lavigne, A.C., Moutahir, F. and Bystrycky, K. (2013) H2A.Z-dependent crosstalk between enhancer and promoter regulates cyclin D1 expression. *Oncogene*, **32**, 4243–4251.
49. Vardabasso, C., Gaspar-Maia, A., Hasson, D., Punzeler, S., Valle-Garcia, D., Straub, T., Keilhauer, E.C., Strub, T., Dong, J., Panda, T. *et al.* (2015) Histone variant H2A.Z.2 mediates proliferation and drug sensitivity of malignant melanoma. *Mol. Cell*, **59**, 75–88.
50. Jan, Y.N. and Jan, L.Y. (2010) Branching out: mechanisms of dendritic arborization. *Nat. Rev. Neurosci.*, **11**, 316–328.
51. Cubelos, B., Sebastian-Serrano, A., Beccari, L., Calcagnotto, M.E., Cisneros, E., Kim, S., Dopazo, A., Alvarez-Dolado, M., Redondo, J.M., Bovolenta, P. *et al.* (2010) Cux1 and Cux2 regulate dendritic branching, spine morphology, and synapses of the upper layer neurons of the cortex. *Neuron*, **66**, 523–535.
52. de Anda, F.C., Rosario, A.L., Durak, O., Tran, T., Graff, J., Meletis, K., Rei, D., Soda, T., Madabhushi, R., Ginty, D.D. *et al.* (2012) Autism spectrum disorder susceptibility gene TAOK2 affects basal dendrite formation in the neocortex. *Nat. Neurosci.*, **15**, 1022–1031.
53. Durak, O., Gao, F., Kaeser-Woo, Y.J., Rueda, R., Martorell, A.J., Nott, A., Liu, C.Y., Watson, L.A. and Tsai, L.H. (2016) Chd8 mediates cortical neurogenesis via transcriptional regulation of cell cycle and Wnt signaling. *Nat. Neurosci.*, **19**, 1477–1488.
54. Watanabe, Y., Khodosevich, K. and Monyer, H. (2014) Dendrite development regulated by the schizophrenia-associated gene FEZ1 involves the ubiquitin proteasome system. *Cell Rep.*, **7**, 552–564.
55. Zovkic, I.B., Paulukaitis, B.S., Day, J.J., Etikala, D.M. and Sweatt, J.D. (2014) Histone H2A.Z subunit exchange controls consolidation of recent and remote memory. *Nature*, **515**, 582–586.
56. Sandberg, M., Flandin, P., Silberberg, S., Su-Feher, L., Price, J.D., Hu, J.S., Kim, C., Visel, A., Nord, A.S. and Rubenstein, J.L.R. (2016) Transcriptional networks controlled by NKX2-1 in the development of forebrain GABAergic neurons. *Neuron*, **91**, 1260–1275.
57. Carvalho, S., Raposo, A.C., Martins, F.B., Grosso, A.R., Sridhara, S.C., Rino, J., Carmo-Fonseca, M. and de Almeida, S.F. (2013) Histone methyltransferase SETD2 coordinates FACT recruitment with nucleosome dynamics during transcription. *Nucleic Acids Res.*, **41**, 2881–2893.